Surface Fluctuating Hydrodynamics Methods for the Drift-Diffusion Dynamics of Particles and Microstructures within Curved Fluid Interfaces

David A. Rower*, Misha Padidar*, and Paul J. Atzberger*

* Department of Mathematics, University of California Santa Barbara; e-mail: atzberg@gmail.com; website: http://atzberger.org/;

We introduce fluctuating hydrodynamics approaches on surfaces for capturing the drift-diffusion dynamics of particles and microstructures immersed within curved fluid interfaces of spherical shape. We take into account the interfacial hydrodynamic coupling, traction coupling with the surrounding bulk fluid, and thermal fluctuations. For fluid-structure interactions, we introduce Immersed Boundary Methods (IBM) and related Stochastic Eulerian-Lagrangian Methods (SELM) for curved surfaces. We use these approaches to investigate the statistics of surface fluctuating hydrodynamics and microstructures. For velocity autocorrelations, we find characteristic power-law scalings τ^{-1}, τ^{-2}, and plateaus can emerge depending on the physical regime associated with the geometry, surface viscosity, and bulk viscosity. This differs from the characteristic $\tau^{-3/2}$ scaling for bulk three dimensional fluids. We develop a theory explaining these observed power-laws that can be interpreted using time-scales associated with dissipation within the fluid interface and coupling to the bulk fluid. We then use our introduced methods to investigate a few example systems including the kinetics of passive particles and active microswimmers. We study how the drift-diffusion dynamics of microstructures compare with and without hydrodynamic coupling within the curved fluid interface.

1. Introduction

Many soft matter systems involve inclusion particles or other microstructures with hydrodynamic interactions mediated through curved fluid interfaces [22, 28, 40]. This includes the motions of proteins within lipid bilayer membranes [2, 4, 40, 69], surfactants and contaminants in bubble interfaces [24, 77], transport in soap films [43, 44], and recent systems with nanoparticles or colloids embedded in fluid interfaces [14, 16, 18, 51, 58, 82, 83]. Related hydrodynamic and curvature mediated phenomena also play an important role in biology and physiology, including transport of surfactants in lung alveoli [39, 54] or in cell mechanics [57, 60, 66]. We develop general approaches to model and simulate the collective drift-diffusion dynamics of particles and other microstructures embedded within curved two-dimensional fluid interfaces. At small length and time scales, thermal fluctuations also play an important role.

We develop methods for curved surfaces building on our prior works on stochastic immersed boundary methods and fluctuating hydrodynamics methods [8, 9, 75]. We also draw on our recent work on developing approaches for deterministic incompressible hydrodynamic flows on curved surfaces [34, 35]. Here, we address how to introduce the spontaneous thermal fluctuations and handle the associated drift-diffusive dynamics of microstructures both in the inertial regime and the quasi-steady regime for the hydrodynamics. We develop theory and computational methods that capture for the fluctuations the correlations arising from the hydrodynamic coupling within the curved fluid interface and from the traction

stresses with the flows of the surrounding bulk fluids.

There has been a lot of work on approaches for investigating hydrodynamic coupling and diffusion based on the classical Saffman-Delbrück (SD) hydrodynamics [72, 73] which were derived for flat viscous sheets [15, 21, 52, 62, 63, 78]. However, in many problems arising in practice the geometry plays an important role as a consequence of significant curvature on the SD length-scale or from the surface topology. These effects can significantly change the hydrodynamic responses relative to the flat case [34, 41, 70, 75]. This has motivated recent work going beyond the classical Saffman-Delbrück theory for flat viscous sheets by formulating hydrodynamic descriptions that take into account the consequences of geometry and additional mechanics arising for curved fluid interfaces [5, 34, 38, 70, 74, 75].

We introduce general fluctuating hydrodynamics methods for the drift-diffusion of particles and microstructures immersed within curved fluid interfaces. To demonstrate ideas, we focus particularly on the case of interfaces of spherical shape. Extending the Saffman-Delbrück theory [72, 73] derived for flat viscous sheets, we formulate hydrodynamic equations for curved fluid interfaces coupled to the surrounding bulk fluid. We introduce thermal fluctuations accounting for the fluid-structure interactions and collective dynamics of the particles and microstructures building on our prior work on stochastic immersed boundary and related methods in [8, 9, 34, 35, 75].

In contrast to the flat Euclidean setting, the curvature of the fluid interface poses significant challenges for immersed boundary methods to obtain appropriate fluid-structure coupling operators for force spreading and velocity averaging [75]. We develop fluid-structure coupling operators that satisfy adjoint conditions to account consistently for inclusion particles within curved surfaces. These operators allow us to derive mobility tensors for the collective hydrodynamic coupling of particles and microstructures within the interface.

The curved geometry and topology of surfaces also pose some additional technical and numerical challenges for generating incompressible hydrodynamic fields with thermal fluctuations. For spherical topologies, this arises in part from the lack of a global coordinate chart. We develop techniques to handle incompressible hydrodynamics based on a generalized vector potential formulation of the fluid mechanics on the surface. In the quasi-steady regime, we further develop techniques based on a formulation of the mobility tensor in the embedding space to derive covariances to capture consistently the hydrodynamic correlations in the fluctuating hydrodynamic fields. Working in the embedding space introduces issues related to the expansion in dimension that results in null spaces for some of the linear operators. We introduce algorithms for stabalization allowing for computation of the stochastic driving forces for the in-plane drift-diffusion dynamics of microstructures within curved surfaces. Our introduced approaches provide in both the inertial and quasi-steady regimes methods that capture in a manner consistent with statistical mechanics the interface hydrodynamics, traction coupling with the surrounding bulk fluid, fluid-structure coupling, and thermal fluctuations.

We organize our paper as follows. We formulate fluctuating hydrodynamic equations and related immersed boundary methods for spherical fluid interfaces in Section 2. We then develop stochastic numerical methods for the drift-diffusion dynamics of particles and microstructures in Section 3. We use our approaches to investigate the statistical mechanics of surface fluctuating hydrodynamics and develop theory for explaining observed power-laws in Section 4. We further demonstrate our approaches by investigating the role of hydrodynamic coupling and related diffusive correlations in the kinetics of passive particles and active microswimmers in Section 4. The results show some of the rich phenomena that can arise and be captured by our introduced fluctu-

ating hydrodynamics approaches for curved fluid interfaces.

2. Fluctuating Hydrodynamics for Curved Fluid Interfaces

In the setting of curved surfaces, physical quantities such as momentum must be treated carefully on the surface with an interpretation referenced to the physical ambient space [56]. This is done by deriving general conservation laws for fluids on curved surfaces by utilizing the invariances of the mechanical energy under different symmetries [34, 56].

2.1. Conservation Laws for Curved Surfaces

The conservation of mass and momentum can be expressed as

$$(1)$$
$$\begin{cases} \rho\dot{\mathbf{v}} & = \overline{\mathrm{div}}\left(\boldsymbol{\sigma}\right) + \rho\bar{\mathbf{b}} \\ \dot{\rho} + \rho\left(\overline{\mathrm{div}}\left(\mathbf{v}_{\parallel}\right) + \mathbf{v}_n H\right) & = 0. \end{cases}$$

The $\mathbf{v}_n$ and $\mathbf{v}_{\parallel}$ denote respectively the components of the fluid velocity normal and tangential to the fluid interface. The H denotes the local mean curvature of the surface [67]. The ρ is the local mass density, $\boldsymbol{\sigma}$ the internal interfacial stress, and $\bar{\mathbf{b}}$ the body force per unit mass.

The $\overline{\mathrm{div}}\left(\mathbf{t}\right) = \mathbf{t}^b_{|b}$ denotes the surface covariant divergence [1, 34, 75]. For a vector field $\mathbf{t} = t^a \partial_{x^a}$ the surface covariant derivative is $\nabla_{\mathbf{w}}\mathbf{t} = t^c_{|b} w^b \partial_{x^c}$ where $t^c_{|b} = \partial t^c / \partial x^b + \Gamma^c_{ab} t^a$ and Γ^c_{ab} denotes the Christoffel symbols [1, 67]. The material derivative of the tensor $\mathbf{t}$ in the manifold setting $\dot{\mathbf{t}} = L_{\mathbf{v}}\mathbf{t}$ corresponds to the Lie derivative of $\mathbf{t}$ under the flow of the velocity field $\mathbf{v}$ [1, 56]. The material derivative of the mass is $\dot{\rho} = \partial\rho/\partial t + \rho\left(\overline{\mathrm{div}}(\mathbf{v}_{\parallel}) + \mathbf{v}_n H\right)$ and the material derivative of the momentum is $\dot{\mathbf{v}} = \partial\mathbf{v}/\partial t + \nabla_{\mathbf{v}}\mathbf{v}$ [1, 34].

Throughout, we shall consider Newtonian incompressible fluid interfaces of fixed shape. In this case, the hydrodynamic flows are tangential to the surface. As a consequence, $\mathbf{v}_n = 0$, $\rho = \rho_0$, $\dot{\rho} = 0$ so that $\overline{\mathrm{div}}\left(\mathbf{v}\right) = 0$. For convenience in our subsequent notation, we supress selectively the $\parallel$ for the velocity $\mathbf{v}$ and the 0 for the density ρ depending on context. We express the conservation laws in this case as

$$\begin{cases} \rho_0\dot{\mathbf{v}} & = \overline{\mathrm{div}}\left(\boldsymbol{\sigma}\right) + \mathbf{b} \\ \overline{\mathrm{div}}\left(\mathbf{v}\right) & = 0. \end{cases} \tag{2}$$

The stress tensor $\boldsymbol{\sigma}$ for an incompressible Newtonian fluid for a curved fluid interface can be expressed as

$$\boldsymbol{\sigma} = \mu_m \mathbf{D} - p\mathcal{I}. \tag{3}$$

The $\mathbf{D}$ is the rate-of-deformation tensor, p is the pressure, and $\mathcal{I}$ is the metric associated identity tensor [56].

Tensors can be expressed in covariant or contravariant form [1, 37]. For vectors in contravariant form we have $\mathbf{t}^{\sharp} = t^a \partial_{x^a}$ or in covariant form $\mathbf{t}^{\flat} = t_a \mathbf{d}x^a$ [1]. The ∂_{x^a} denotes the ath coordinate basis vector. The $\mathbf{d}x^a$ denotes the ath coordinate basis covector (differential 1-form) with $\mathbf{d}x^a[\partial_{x^b}] = \delta^b_a$ [1]. We can convert between vectors and covectors by the mappings $\flat : t^a \to t_a = g_{ab}t^b$ and $\sharp : t_a \to t^a = g^{ab}t_b$. The g_{ab} denotes the metric tensor and g^{ab} the inverse metric tensor [1]. These maps $\flat$ and $\sharp$ between the tangent space and cotangent space correspond to lowering and raising indices in the coordinate expressions of the tensors [1, 37].

We find it convenient in our calculations to express tensors in covariant form and use exterior calculus [1]. This allows us to generalize vector calculus and many techniques employed for fluid mechanics to the manifold setting [34, 35, 75]. For an incompressible Newtonian fluid interface, the stress $\boldsymbol{\sigma}$ is given in equation 3. The divergence of the stress tensor on the surface $\overline{\mathrm{div}}\left(\boldsymbol{\sigma}\right)$ becomes in covariant form [34, 56, 75]

$$\overline{\mathrm{div}}\left(\boldsymbol{\sigma}\right)^{\flat} = \mu_m\left(-\boldsymbol{\delta}\mathbf{d}\mathbf{v}^{\flat} + 2K\mathbf{v}^{\flat}\right) - \mathbf{d}p. \tag{4}$$

The **d** is the exterior derivative playing here a role similar to the gradient on the surface, $\boldsymbol{\delta}$ is the co-differential playing a role similar to the divergence on the surface, and K is the Gaussian curvature of the surface [1, 67].

2.2. Fluctuating Hydrodynamics with Fluid-Structure Interactions

We introduce a fluctuating hydrodynamics description to account for the drift-diffusion motions of microstructures and their hydrodynamic coupling [8, 9, 75]. In covariant form, we introduce for curved fluid interfaces fluctuating hydrodynamic equations incorporating fluid-structure interactions. We show a schematic of our general approach in Figure 1.

The fluid dynamics are modeled by

$$
\begin{aligned}
\rho \frac{d\mathbf{v}^\flat}{dt} &= \mu_m \left(-\boldsymbol{\delta}\mathbf{d}\mathbf{v}^\flat + 2K\mathbf{v}^\flat \right) - \mathbf{d}p \quad (5)\\
&+ \mathbf{t}^\flat \\
&+ \Lambda \left[\gamma \left(\mathbf{V} - \Gamma\mathbf{v}^\flat \right) \right] + \mathbf{f}^\flat_{thm} \\
-\boldsymbol{\delta}\mathbf{v}^\flat &= 0. \quad (6)
\end{aligned}
$$

The drift-diffuson motions of microstructures are modeled by

$$
\begin{aligned}
m \frac{d\mathbf{V}}{dt} &= -\gamma \left(\mathbf{V} - \Gamma\mathbf{v}^\flat \right) - \nabla\phi + \mathbf{F}_{thm} \quad (7)\\
\frac{d\mathbf{X}}{dt} &= \mathbf{V}. \quad (8)
\end{aligned}
$$

The $\mathbf{v}^\flat$ denotes the fluid velocity. The $\mathbf{X}$ and $\mathbf{V}$ denotes the collective configuration and velocity of the microstructures immersed within the fluid. The μ_m is the fluid shear viscosity, p is the pressure. As is commonly done in fluctuating hydrodynamics, we neglect the typically lower-order advection term contributions in equation 5 given the rapid oscillations of the fluid from the thermal fluctuations [79]. The Λ and Γ are fluid-structure coupling operators we shall discuss in more detail in Section 2.5. The γ is the drag coupling coefficient between microstructures and the fluid, $-\nabla\phi$ are the conservative forces acting on microstructures, and $\mathbf{f}_{thm}$ and $\mathbf{F}_{thm}$ are stochastic forces accounting for thermal fluctuations of the system.

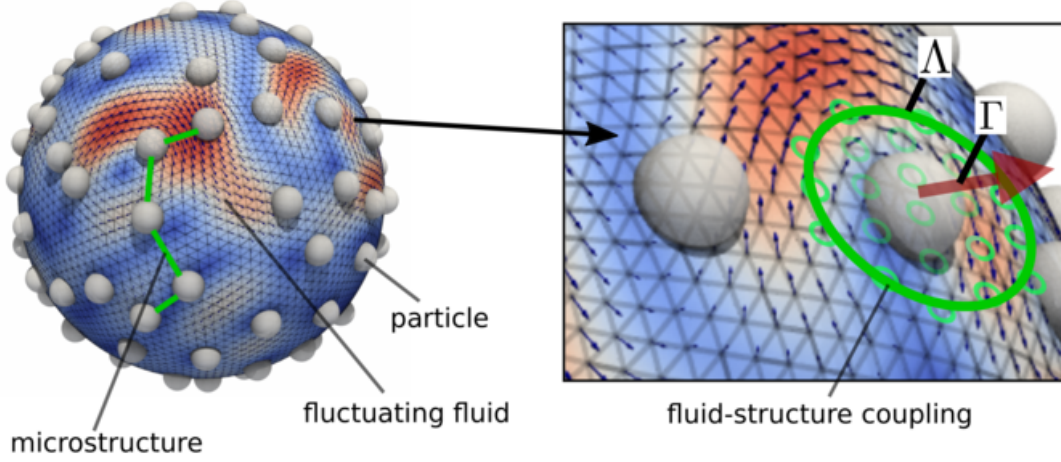**Surface Fluctuating Hydrodynamics with Fluid-Structure Interactions**

Figure 1: *Surface Fluctuating Hydrodynamics with Fluid-Structure Interactions. To model particles and microstructures embedded in curved fluid interfaces, we couple a Lagrangian description of the microstructures to an Eulerian description for the fluid mechanics. The coupling is modeled by the two operators Γ and Λ. The operator Γ gives a kinematic reference fluid velocity used to determine how the fluid exerts force upon microstructures in equation 7. The operator Λ gives the related force density for how the microstructures exert force on the fluid in equation 5. We model the drift-diffusion dynamics of microstructures by the SELM fluctuating hydrodynamics description introduced in equations 5 - 8.*

2.3. Traction Stress from Flow of the Surrounding Bulk Fluid

For the spherical geometry, we use Lamb's solution [36, 46] to obtain the traction stresses $\mathbf{t}^{\flat} = \mathcal{T}_f \mathbf{v}^{\flat}$ that arises from $\mathbf{v}$ in entraining flow of the surrounding bulk fluid [75]. Our approach here makes the assumption that the bulk surrounding flow arises from an incompressible Newtonian fluid that reaches steady-state rapidly when contributing to the surface traction. Let the bulk fluid velocity be denoted by $\mathbf{u}$ with values on the surface $\mathbf{u} = \mathbf{v} + v_n \mathbf{n}$, where we shall assume $v_n = 0$ throughout. The solution can be expressed using the spherical harmonics expansion

$$\mathbf{r} \cdot \nabla \times \mathbf{u} \;\; = \;\; \sum_{\ell=-\infty}^{\infty} Z_\ell. \tag{9}$$

We emphasize here the curl $\nabla\times$ is the usual operator in three dimensional Euclidean space. The

Z_ℓ denotes the combined contributions of all of the solid spherical harmonic terms of degree ℓ. We also expand the bulk surrounding fluid flows inside the sphere $\mathbf{u}^-$ and outside the sphere $\mathbf{u}^+$ as

$$\mathbf{u}^+ = \sum_{\ell=0}^{\infty} \mathbf{u}_\ell^+, \;\; \mathbf{u}^- = \sum_{\ell=1}^{\infty} \mathbf{u}_\ell^-. \tag{10}$$

The $\mathbf{u}_\ell^+$ and $\mathbf{u}_\ell^-$ are the solid spherical harmonic expansion terms combined for degree ℓ. The Lamb solutions for the bulk fluid velocity fields are given by [36, 46]

$$\mathbf{u}_\ell^+ = \nabla \times \left(\mathbf{r} \chi_{-(\ell+1)} \right), \;\; \mathbf{u}_\ell^- = \nabla \times \left(\mathbf{r} \chi_\ell \right) \tag{11}$$

where

$$\chi_\ell \;\; = \;\; \frac{1}{\ell(\ell+1)} \left(\frac{r}{R} \right)^\ell Z_\ell \tag{12}$$

$$\chi_{-(\ell+1)} \;\; = \;\; \frac{1}{\ell(\ell+1)} \left(\frac{R}{r} \right)^{\ell+1} Z_\ell. \tag{13}$$

The traction stress in contravariant form $\mathbf{t}^{\sharp} = \mathbf{t}^{+} + \mathbf{t}^{-}$ is

$$\mathbf{t}^{+} = \boldsymbol{\sigma}^{+} \cdot \mathbf{n}^{+} = \mu_{+}\frac{\partial \mathbf{u}^{+}}{\partial r} + \mu_{+}\nabla\left(\mathbf{u}^{+} \cdot \mathbf{n}^{+}\right) \quad (14)$$

$$\mathbf{t}^{-} = \boldsymbol{\sigma}^{-} \cdot \mathbf{n}^{-} = -\mu_{-}\frac{\partial \mathbf{u}^{-}}{\partial r} + \mu_{-}\nabla\left(\mathbf{u}^{-} \cdot \mathbf{n}^{-}\right). (15)$$

We emphasize in the above notation $\mathbf{n}$ is evaluated at the fixed location of traction on the surface and does not change when taking the gradient ∇. The $\boldsymbol{\sigma}^{\pm}$ is the the fluid shear stress and pressure from the bulk surrounding fluid arising at the fluid interface. We take $\mu_{\pm} = \mu_f$ throughout. The traction can be expressed in terms of the spherical harmonics expansion as

$$\mathbf{t}^{+} = -\mu_{+}\sum_{\ell=0}^{\infty}\frac{(\ell+2)}{R}\mathbf{u}_{\ell}^{+} =: \tilde{\mathcal{T}}_{f}^{+}\mathbf{v}^{\sharp} \quad (16)$$

$$\mathbf{t}^{-} = -\mu_{-}\sum_{\ell=1}^{\infty}\frac{(\ell-1)}{R}\mathbf{u}_{\ell}^{-} =: \tilde{\mathcal{T}}_{f}^{-}\mathbf{v}^{\sharp}. \quad (17)$$

The bulk fluid flow has $\mathbf{u}^{+} = \mathbf{u}^{-} = \mathbf{v}$ on the fluid interface and is completely determined by $\mathbf{v}$. We define in covariant form the traction operators on the surface corresponding to equation 16 and 17 as $\mathbf{t}^{\flat} = \mathcal{T}_{f}\mathbf{v}^{\flat} = \mathcal{T}_{f}^{+}\mathbf{v}^{\flat} + \mathcal{T}_{f}^{-}\mathbf{v}^{\flat}$.

2.4. Thermal Fluctuations

To determine the associated stochastic driving terms $\mathbf{f}_{thm}(\mathbf{x}, t)$ and $\mathbf{F}_{thm}(t)$ that account for thermal fluctuations, we use an approach related to our Stochastic Eulerian Lagrangian Method (SELM) framework [9, 79]. We use this in the setting of the curved fluid interface to derive stochastic driving terms $\mathbf{f}_{thm}(\mathbf{x}, t)$ and $\mathbf{F}_{thm}(t)$. These are introduced as Gaussian processes that are δ-correlated in time with mean zero and covariances

$$\left\langle \mathbf{f}_{thm}(t)\mathbf{f}_{thm}(s)^{T}\right\rangle = -2k_{B}T\mathcal{L}_{ff}\delta(t-s) \quad (18)$$
$$\left\langle \mathbf{F}_{thm}(t)\mathbf{F}_{thm}(s)^{T}\right\rangle = 2k_{B}T\gamma\mathcal{I}\delta(t-s) \quad (19)$$
$$\left\langle \mathbf{F}_{thm}(t)\mathbf{f}_{thm}(s)^{T}\right\rangle = -2k_{B}T\gamma\Gamma\delta(t-s). \quad (20)$$

Here, the $\langle\cdot\rangle$ is to be interperted as an expectation average taken over the probability distribution.

The first term involves the dissipative operator associated with the fluid $\mathcal{L}_{ff}\mathbf{v}^{\flat}$ where

$$\mathcal{L}_{ff} = \mathcal{L}_{f} - \gamma\Lambda\Gamma \quad (21)$$
$$\mathcal{L}_{f} = \mu_{m}\left(-\boldsymbol{\delta}\mathbf{d} + 2K\right) + \mathcal{T}_{f}. \quad (22)$$

The second term arises from the dissipative term of the microstructure degrees of freedom $\mathcal{L}_{p}\mathbf{V} = -\gamma\mathcal{I}\mathbf{V}$. The third term gives the cross-correlation that arises from the coupling terms $\mathcal{L}_{fp}\mathbf{V} = \gamma\Lambda\mathbf{V}$ and $\mathcal{L}_{pf}\mathbf{v}^{\flat} = \gamma\Gamma\mathbf{v}^{\flat}$.

We shall also find it useful to express these thermal fluctuations using $\mathbf{g}_{thm}$ which we take to be independent of $\mathbf{F}_{thm}$ with covariance

$$\left\langle \mathbf{g}_{thm}(t)\mathbf{g}_{thm}(s)^{T}\right\rangle = -2k_{B}T\mathcal{L}_{f}\delta(t-s). \quad (23)$$

We can then express the thermal fluctuations for the hydrodynamics as $\mathbf{f}_{thm} = \mathbf{g}_{thm} - \Lambda[\mathbf{F}_{thm}]$ to obtain the needed correlations.

Here, we have used that the fluid-structure coupling operators are adjoints $\Lambda = \Gamma^{T}$ in the sense $\int_{\mathcal{S}}\langle\Lambda\mathbf{U}, \mathbf{u}^{\flat}\rangle_{g}dA = \langle\mathbf{U}, \Gamma\mathbf{u}^{\flat}\rangle$ for all choices of $\mathbf{U}$ and $\mathbf{u}^{\flat}$ [9, 75]. We discuss choices for the coupling operators and the adjoint conditions in more detail in Section 2.5. For the stochastic driving terms of equations 5– 8 and 18– 20, our SELM approach ensures when the system is at thermodynamic equilibrium that the Gibbs-Boltzmann distribution is invariant under the stochastic dynamics and satisfies detailed-balance [9, 71, 79]. The stochastic equations 5– 8 should be interpreted in the sense of Ito Calculus [30, 61].

We remark that the covariance operators in equations 18–20 are to be interpreted in the weak sense [9, 11, 53]. Consider $\mathbf{u}(\mathbf{x}) = \int\int\boldsymbol{\alpha}(\mathbf{z}, r, \mathbf{x})^{T}\mathbf{f}_{thm}(\mathbf{z}, r)d\mathbf{z}dr$ and $\tilde{\mathbf{u}}(\mathbf{y}) = \int\int\tilde{\boldsymbol{\alpha}}(\mathbf{w}, q, \mathbf{y})^{T}\mathbf{f}_{thm}(\mathbf{w}, q)d\mathbf{w}dq$ and $\mathbf{U} = \int\mathbf{A}(r)^{T}\mathbf{F}_{thm}(r)dr$ and $\tilde{\mathbf{U}} = \int\tilde{\mathbf{A}}(q)^{T}\mathbf{F}_{thm}(q)dq$. The $\boldsymbol{\alpha}$, $\tilde{\boldsymbol{\alpha}}$, $\mathbf{A}$, $\tilde{\mathbf{A}}$ are smooth fields and vectors playing the role of test functions. [53]. The asso-

ciated covariances are

$$\langle \mathbf{u}(\mathbf{x})\tilde{\mathbf{u}}(\mathbf{y})^T \rangle = \qquad (24)$$

$$-\int\int\int\int \boldsymbol{\alpha}(\mathbf{z}, r, \mathbf{x})^T 2k_B T \mathcal{L}_{ff} \tilde{\boldsymbol{\alpha}}(\mathbf{w}, q, \mathbf{y}) d\mathbf{w} d\mathbf{z} \cdot$$
$$\delta(r - q) dr dq.$$

Here, the differential operator $\mathcal{L}_{ff}$ acts in the parameter $\mathbf{w}$. We also have the covariances

$$\qquad (25)$$

$$\langle \mathbf{U}\tilde{\mathbf{U}}^T \rangle = \int\int 2k_B T \gamma \mathbf{A}(r)^T \tilde{\mathbf{A}}(q) \delta(r - q) dr dq,$$

and

$$\qquad (26)$$

$$\langle \mathbf{U}\tilde{\mathbf{u}}(\mathbf{y})^T \rangle = -\int\int\int 2k_B T \gamma \mathbf{A}(r)^T \Gamma \tilde{\boldsymbol{\alpha}}(\mathbf{w}, q, \mathbf{y}) \cdot$$
$$\delta(r - q) d\mathbf{w} dr dq.$$

Here, the operator Γ acts in the parameter $\mathbf{w}$. Additional discussions on how to interpret these operator covariances also can be found in [9, 11].

2.5. Fluid-Structure Coupling: Immersed Boundary Methods for Curved Surfaces

We handle the fluid-structure interactions between the particles and microstructures with the fluid by developing extended immersed boundary methods in the manifold setting [8, 9, 65], see Figure 1. Many choices can be made for the operators Γ and Λ [9]. To ensure that the approximate fluid-structure coupling which converts between the Eulerian and Lagrangian reference frames are non-dissipative, the operators are taken to be adjoints [9, 65, 79].

We require the coupling operators satisfy the following adjoint conditions for any choice of test field $\mathbf{v}$ and vector $\mathbf{F}$

$$\langle \Gamma \mathbf{v}, \mathbf{F} \rangle = \langle \mathbf{v}, \Lambda \mathbf{F} \rangle, \qquad (27)$$

where the inner-products are defined as

$$\langle \Gamma \mathbf{v}, \mathbf{F} \rangle = \sum_i [\Gamma \mathbf{v}]_i \cdot [\mathbf{F}]_i \qquad (28)$$

$$\langle \mathbf{v}, \Lambda \mathbf{F} \rangle = \int_\Omega \mathbf{v}(\mathbf{x}) \cdot (\Lambda \mathbf{F})(\mathbf{x}) d\mathbf{x}. \qquad (29)$$

The $\mathbf{X}$ denotes the collective vector of particle locations. The ith particle is at location $[\mathbf{X}]_i$. The $\cdot$ denotes the vector dot-product induced by the ambient physical space. For vector fields on the surface $\mathbf{v}$ and $\mathbf{u}$ we have $\mathbf{v}(\mathbf{x}) \cdot \mathbf{u}(\mathbf{x}) = \langle \mathbf{v}(\mathbf{x}), \mathbf{v}(\mathbf{x}) \rangle_g = v^a g_{ab} u^b$. We use the notation $\Gamma^T = \Lambda$ to denote the adjoint condition 27.

In the setting of curved surfaces the coupling operators Γ and Λ must be chosen carefully so that velocity averaging occurs over the surface and so that force densities provide well-controlled components in the directions of the normal and tangent space of the surface. We develop operators of the form

$$\Gamma \mathbf{v} = \int_\Omega \mathbf{W}[\mathbf{v}](\mathbf{y}) d\mathbf{y} \qquad (30)$$

$$\Lambda \mathbf{F} = \mathbf{W}^*[\mathbf{F}](\mathbf{x}). \qquad (31)$$

We use a tensor $\mathbf{W}$ to sample and weight values on the surface to perform velocity averaging. We use the adjoint tensor $\mathbf{W}^*$ to produce a corresponding force density field on the surface compatible with our adjoint conditions 27. For the curved surface, we use the geometrically motivated forms

$$\mathbf{W}[\mathbf{v}] = \sum_i \mathbf{w}^{[i],\alpha}[\mathbf{v}] \partial_{x^\alpha}|_{\mathbf{X}^{[i]}} \qquad (32)$$

$$\mathbf{W}^*[\mathbf{F}] = \sum_i \left(w^{[i],\alpha} \right)^\gamma F^\alpha \partial_{x^\gamma}. \qquad (33)$$

The sum i runs over the particle indices and the $\partial_{x^\alpha}|_{\mathbf{X}^{[i]}}$ denotes the tangent basis vector in direction α at location $\mathbf{X}^{[i]}$. We refer to the vector field $\mathbf{w}^{[i],\alpha}$ as the probing vector field for direction α.

On the sphere, we have a lot of symmetry that can be utilized. For this case with the spherical

coordinates (θ, ϕ), we take our probing vector fields to be of the form $\mathbf{w}^{[i],\theta} = \psi(\mathbf{x} - \mathbf{X}^{[i]})\partial_\theta$ and $\mathbf{w}^{[i],\phi} = \left(\psi(\mathbf{x} - \mathbf{X}^{[i]})/\cos(\theta)\right)\partial_\phi$, where $\psi(r) = C\exp(-r^2/2\sigma^2)$. In practice, we truncate at length $r_0 = 4\sigma$ and use C to normalize so that $\psi(r)$ averages to one on the surface.

2.6. Overdamped Limit

In physical regimes corresponding to small Reynolds numbers $Re \ll 1$ we can consider the overdamped limit of the the fluctuating hydrodynamic equations 5– 7 [9, 79]. In this regime the limiting fluctuating hydrodynamic equations can be expressed as

$$\frac{d\mathbf{X}}{dt} = \mathbf{MF} + k_B T \nabla \cdot \mathbf{M} + \mathbf{F}_{thm} \qquad (34)$$

$$\langle \mathbf{F}_{thm}(s)\mathbf{F}_{thm}(t)^T \rangle = 2k_B T \mathbf{M}\delta(t - s)$$

where

$$M \;=\; \gamma^{-1}\mathcal{I} + \Gamma\mathcal{S}\Lambda. \qquad (35)$$

Here, we take the overdamped limit while retaining the finite slip term $-\gamma\left(\mathbf{V} - \Gamma\mathbf{v}^\flat\right)$ in equation 5 and 7 resulting in the term $\gamma^{-1}\mathcal{I}$ in equation 35 [79]. In the strong-coupling limit $\gamma \to \infty$ the mobility simplifies to

$$M \;=\; \Gamma\mathcal{S}\Lambda. \qquad (36)$$

The velocity averaging operator Γ and force spreading operator Λ are as discussed in Section 2.5. The $\mathcal{S}$ denotes the solution operator giving $\mathbf{v}^\flat = \mathcal{S}\mathbf{b}^\flat$ for the following hydrodynamic equations

$$(\mu_m(-\boldsymbol{\delta}\mathbf{d} + 2K) + \mathcal{T}_f)\,\mathbf{v}^\flat = -\mathbf{b}^\flat \qquad (37)$$

$$-\boldsymbol{\delta}\mathbf{v}^\flat = 0. \qquad (38)$$

The $\mathcal{T}_f$ corresponds to the traction stresses with the surrounding bulk fluid as discussed in Section 2.2. The $\mathbf{v}^\flat = \mathcal{S}\Lambda\mathbf{F}$ corresponds to the case with $\mathbf{b} = \Lambda[\mathbf{F}]$ where in practice we will typically have $\mathbf{F} = -\nabla\phi$.

To simply expressions we have also taken here for equation 34 the limit of no-slip between the microstructure and the fluid which corresponds formally to $\gamma/m \to \infty$. This yields $d\mathbf{X}/dt = \mathbf{V} = \Gamma\mathbf{v}^\flat$ throughout. Putting this together we arrive at the first term in equation 34. For the full stochastic system, we perform related detailed dimensional analysis and asymptotics in [9, 75, 79]. In this physical regime, when equation 34 is given the Ito interpretation, the thermal fluctuations involve configuration dependent correlations resulting in the spontaneous drift term $k_B T \nabla \cdot \mathbf{M}$ [9, 30, 61, 79]. Additional analysis of the Stochastic Eulerian Lagrangian Methods (SELM) and related regimes can be found in [9, 75, 79].

2.7. Formulating Fluctuating Hydrodynamics on Surfaces using Vector Potentials Φ

The hydrodynamic responses both in the inertial fluctuating hydrodynamics of equation 5 and in the overdamped regime of equation 37 require computation of the operator $\mathcal{L}_f$ of equation 22. Since the hydrodynamic fields are incompressible, we can use the Hodge decomposition of the fluid velocity $\mathbf{v}^\flat = \mathbf{d}\tilde{\Phi} + \boldsymbol{\delta}\Psi + h$ where $\Delta_H = \mathbf{d}\boldsymbol{\delta} + \mathbf{d}\boldsymbol{\delta}$ is the Hodge Laplacian and h is harmonic in the sense $\Delta_H h = 0$. Using this in the case of spherical geometry with velocity tangential to the surface, we can express any incompressible flow as $\mathbf{v}^\flat = -\star\mathbf{d}\Phi$ [75]. This allows us to reformulate the inertial hydrodynamics of equation 5 in terms of Φ as

$$\rho\Delta_{LB}\frac{\partial\Phi(t)}{\partial t} = (-\star\mathbf{d})\mathcal{L}_f(-\star\mathbf{d}) - \star\mathbf{d}\mathbf{b}^\flat$$

$$= \mu_m\Delta_{LB}^2\Phi - 2\star\mathbf{d}\mu_m K(-\star\mathbf{d})\Phi$$

$$- \star\mathbf{d}\mathcal{T}_f(-\star\mathbf{d})\Phi - \star\mathbf{d}\mathbf{b}^\flat$$

$$= \Delta_{LB}\left(\tilde{\mathcal{L}}_f\Phi + c\right). \qquad (39)$$

The $\mathbf{b}^\flat = -\star\mathbf{d}c$ denotes all of the forces acting on the fluid. The $\Delta_{LB} = -\boldsymbol{\delta}\mathbf{d}$ denotes the Laplace-Beltrami operator [1]. The $\mathcal{T}_f$ denotes

the traction stress operator of equation 14 and 15. The $\mathcal{L}_f$ denotes the operator in equation 22 capturing the hydrodynamic response.

We obtained equation 39 by substituting for Φ using $\mathbf{v}^\flat = - \star \mathbf{d}\Phi$ and then taking the generalized curl $- \star \mathbf{d}$ of both sides. We also used that the generalized curl commutes with the operator $\mathcal{L}_f$ in the sense $(- \star \mathbf{d})\mathcal{L}_f(- \star \mathbf{d}) = \Delta_{LB}\tilde{\mathcal{L}}_f$ where $\tilde{\mathcal{L}}_f$ takes on a form similar to equation 22 but now applied to scalar fields. We provide more details for $\tilde{\mathcal{L}}_f$ in terms of spherical harmonic coefficients below. These considerations allow for the fluctuating hydrodynamics to be expressed as

$$\rho\frac{\partial\Phi(t)}{\partial t} = \tilde{\mathcal{L}}_f\Phi + c.$$

In the overdamped regime, we need to compute the mobility tensor $M(\mathbf{X})$ of the hydrodynamic coupling in equation 35. This requires us to solve the steady-state hydrodynamic equations 37 which can be reformulated as

$$\mu_m\Delta_{LB}^2\Phi - 2 \star \mathbf{d}\mu_m K(- \star \mathbf{d})\Phi$$
$$- \star \mathbf{d}\mathcal{T}_f(- \star \mathbf{d})\Phi = \star\mathbf{d}\mathbf{b}^\flat. \qquad (40)$$

We use again that the generalized curl commutes with the operator $\mathcal{L}_f$ in the sense $(- \star \mathbf{d})\mathcal{L}_f(- \star \mathbf{d}) = \Delta_{LB}\tilde{\mathcal{L}}_f$. This yields for the steady-state hydrodynamics

$$\tilde{\mathcal{L}}_f\Phi = -c.$$

Central to both the inertial fluctuating hydrodynamics and steady-state regimes is computation of the action of the operator $\tilde{\mathcal{L}}_f\Phi$ which captures the hydrodynamic responses of the system. We expand Φ using spherical harmonics to represent the vector potential as $\Phi = \sum_s \Phi_s = \sum_s a_s Y_s$ where $\Phi_s = a_s Y_s$ and $s = (\ell, m)$ denotes the spherical harmonics index, see Appendix C. For the spherical geometry, we can express solutions using that the spherical harmonics are eigenfunctions of the Laplace-Beltrami operator [34, 75].

The action of the operator can be expressed as

$$\tilde{\mathcal{L}}_f\Phi_s = \Delta_{LB}^{-1}(- \star \mathbf{d})\mathcal{L}_f(- \star \mathbf{d})\Phi_s = L_s a_s Y_s, (41)$$

where

$$L_s = \frac{\mu_m}{R^2}\left[2 - \ell(\ell + 1) + \right. \qquad (42)$$
$$\left. -\frac{R}{L^+}(\ell + 2) - \frac{R}{L^-}(\ell - 1)\right],$$

with $L^\pm = \mu_m/\mu_\pm$. In the case with $\mu_\pm = \mu_f$ this can be simplified to

$$L_s = \frac{\mu_m}{R^2}\left[2 - \ell(\ell + 1) - \frac{R}{L}\left(\ell + \frac{1}{2}\right)\right] \quad (43)$$

where $L = \mu_m/(\mu_+ + \mu_i) = \mu_m/2\mu_f$. We see from this that the hydrodynamic flow on the sphere is characterized by the non-dimensional parameter $\Pi_1 = L/R$, where $L = \mu_m/2\mu_f$ is the Saffman-Delbrück length-scale [73] and R the radius of the sphere.

In the overdamped regime to obtain the steady-state hydrodynamics, we can solve the hydrodynamic equations to obtain directly the spherical harmonics coefficients as

$$a_s = L_s^{-1}c_s. \qquad (44)$$

For the inertial fluctuating hydrodynamics of equation 5 and equation 39, we can express the dynamics in terms of the spherical harmonics coefficients a_s as

$$(45)$$
$$\frac{\partial a_s(t)}{\partial t} = \rho^{-1}L_s a_s(t) + \rho^{-1}\bar{c}_s(t) + g_s(t) + h_s(t),$$

where $c_s = \bar{c}_s + g_s + h_s$. The stochastic driving terms $\{g_s\}$ as associated with the hydrodynamics and are complex-valued Gaussian processes δ-correlated in time with mean zero and covariance

$$(46)$$
$$\left\langle g_s(t)\overline{g_{s'}(r)}\right\rangle = -2k_BT\rho^{-2}|\lambda_s|^{-1}L_s\delta_{ss'}\delta(t - r).$$

The stochastic driving terms $\{h_s\}$ are associated with the fluid-structure coupling discussed in Section 2.5 that contributes dissipation to the system

through $\bar{c}$, see equation 5. The h_s are complex-valued Gaussian processes having correlations with the microstructure stochastic dynamics in equation 7 which we can express as

$$h_s(t) = \hspace{5cm} (47)$$
$$-\rho^{-1} \left\langle \Delta_{LB}^{-1}(-\star \mathbf{d})\Lambda[\mathbf{F}_{thm}(t)](\mathbf{x}), Y_s(\mathbf{x})\right\rangle_{L^2}.$$

The $\lambda_s = -\ell(\ell+1)/R^2$ denotes the sth eigenvalue of the Laplace-Beltrami operator $\Delta_{LB} = -\boldsymbol{\delta}\mathbf{d}$. The $\delta_{a,b}$ denotes the Kronecker δ-function which is zero for $a \neq b$ and one for $a = b$.

The real-space fluctuating velocity field $\mathbf{v}^\flat$ can be recovered using $\mathbf{v} = (-\star \mathbf{d}\Phi)^\sharp$. This is derived from the stochastic force $\mathbf{F}_{thm}$ acting on microstructures in equation 7. Together, these stochastic driving terms give in real-space $\mathbf{f}_{thm}^\flat = -\star \mathbf{d}\sum_s \rho(g_s + h_s)Y_s = \mathbf{g}_{thm}^\flat - \Lambda[\mathbf{F}_{thm}]$ which satisfy equations 18–20.

In summary, the equations 45– 47 give a formulation of the SELM fluctuating hydrodynamics incorporating fluid-structure interactions in terms of the vector potential Φ. The use of such Hodge decompositions and vector potentials is particularly convenient when representing velocity fields on surfaces. We give additional details on the derivation of these results in Appendix A.

3. Stochastic Numerical Methods

We develop numerical methods for the drift-diffusion dynamics of microstructures both in the inertial and over-damped regimes. To handle the incompressibility constraint for the surface hydrodynamics we make use of our generalized vector potential formulation discussed in Section 2.7.

3.1. Inertial Regime

In the inertial regime, we formulate the time-step integration of the fluctuating hydrodynamics of equation 5 in terms of stochastic dynamics of the vector potential Φ in equation 39 and 45. We use the time-step update in terms of the spherical harmonics coefficients of Φ,

$$a_s^{n+1} = a_s^n + \Delta t\rho^{-1}L_s a_s^n + \Delta t\rho^{-1}c_s^n + g_s^n + h_s^n. \hspace{0.5cm} (48)$$

For the microstructure dynamics, we use the update

$$
\begin{aligned}
\mathbf{V}^{n+1/2} &= \mathbf{V}^n - \frac{\Delta t}{2m}\gamma(\mathbf{V}^n - \Gamma^n\mathbf{v}^n) + \frac{\Delta t}{2m}\mathbf{F}_{thm}^n \\
&\quad + \frac{\Delta t}{2m}\mathbf{F}^n \\
\mathbf{X}^{n+1} &= \mathbf{X}^n + \Delta t\mathbf{V}^{n+1/2} \\
\mathbf{V}^{n+1} &= \mathbf{V}^n - \frac{\Delta t}{2m}\gamma(\mathbf{V}^n - \Gamma^n\mathbf{v}^n) + \frac{\Delta t}{2m}\mathbf{F}_{thm}^n \\
&\quad + \frac{\Delta t}{2m}\mathbf{F}^{n+1}.
\end{aligned}
\hspace{0.5cm} (49)
$$

We have $\Phi^n = \sum_s a_s^n Y_s$ with the fluid velocity obtained by $\mathbf{v}^n = (-\star\mathbf{d}\Phi^n)^\sharp$. Similarly, from the fluid-structure coupling $\mathbf{c}^n = \Lambda^n[\gamma(\mathbf{V}^n-\Gamma^n\mathbf{v}^n]$ we obtain the terms $c_s^n = \left\langle \Delta_{LB}^{-1}(-\star\mathbf{d})\mathbf{c}^n, Y_s(\mathbf{x})\right\rangle_{L^2}$.

We account for thermal fluctuations of the microstructures over the time-step through the Gaussian term $\mathbf{F}_{thm}^n$. This has mean zero and covariance

$$\left\langle \mathbf{F}_{thm}^n \mathbf{F}_{thm}^m \right\rangle = 2k_B T\gamma\Delta t^{-1}\delta_{m,n}. \hspace{0.5cm} (50)$$

The g_s^n are complex-valued Gaussians with mean zero and covariance

$$\left\langle g_s^n g_{s'}^m \right\rangle = -2\rho^{-1}L_s \mathcal{C}_{ss'}\Delta t\delta_{nm}. \hspace{0.5cm} (51)$$

The L_s are given by equation 43 or 42 and $\mathcal{C}_{ss'}$ are the equilibrium fluctuations of the modes a_s given by

$$\mathcal{C}_{ss'} = \left\langle a_s a_{s'} \right\rangle = \rho^{-1}k_B T|\lambda_s|^{-1}\delta_{s',\bar{s}}. \hspace{0.5cm} (52)$$

The $\lambda_s = -\ell(\ell+1)/R^2$ are the eignvalues of the Laplace-Beltrami operator $\Delta_{LB} = -\boldsymbol{\delta}\mathbf{d}$ on the surface. For $s = (\ell, m)$ the $\bar{s} = (\ell, -m)$.

The h_s^n are complex-valued Gaussians which we generate from $\mathbf{F}_{thm}^n$ by

$$h_s^n = \hspace{5cm} (53)$$
$$-\rho^{-1}\Delta t \left\langle \Delta_{LB}^{-1}(-\star\mathbf{d})\Lambda^n[\mathbf{F}_{thm}^n](\mathbf{x}), Y_s(\mathbf{x})\right\rangle_{L^2}.$$

This ensures proper correlations in the system between the microstructure and the fluctuating hydrodynamics. We note that in our derivation of $\mathbf{F}_{thm}$ there were negative cross correlations with the fluid which we capture in our numerical methods consistent with equation 20. These cross-correlations play the important role of ensuring momentum conservation. They account for the spontaneous fluctuations that exchange momentum back and forth between the fluid and microstructures.

The integrator approach we have introduced works well when the time-scales are comperable between the microstructure evolution and hydrodynamics. When there is a disparity in these time-scales, stiff stochastic numerical time-step integrators can also be developed using our vector potential formulation. For instance, we can develop exponential time-stepping approaches similar to our prior works [8,85]. As an alternative, an asymptotic analysis of the stochastic dynamics of the fluid-structure system can also be performed as in [79]. This can be used to formulate equations in over-damped regimes and develop numerical methods for the drift-diffusion dynamics of the microstructures [79].

3.2. Overdamped Regime

For the overdamped regime, we develop numerical methods for simulations based on a stochastic variant of the Velocity-Verlet method [27, 81]. We account for the thermal drift term in the stochastic dynamics using an approach related to methods proposed in [20, 25]. We update the collective configuration $\mathbf{X}$ of the particles or mi-crostructures of the system using

$$\mathbf{V}^n = M(\mathbf{X}^n)\mathbf{F}^n + Q(\mathbf{X}^n)\boldsymbol{\xi}^n$$
$$\tilde{\mathbf{X}}^{n+1} = \mathbf{X}^n + \mathbf{V}^n\Delta t$$
$$\tilde{\mathbf{V}}^{n+1} = M(\tilde{\mathbf{X}}^{n+1})\tilde{\mathbf{F}}^{n+1} + Q(\mathbf{X}^n)\boldsymbol{\xi}^n$$
$$\mathbf{X}^{n+1} = \frac{1}{2}\left(\mathbf{V}^n + \tilde{\mathbf{V}}^{n+1}\right)\Delta t$$
$$+ k_B T\left(\frac{\Delta t}{\delta}\right)\left\langle\left(M\left(\mathbf{X}^n + \delta\hat{\boldsymbol{\xi}}\right) - M\left(\mathbf{X}^n\right)\right)\hat{\boldsymbol{\xi}}\right\rangle_{\bar{N}}.$$

(54)

The thermal fluctuations have correlations generated by $Q(\mathbf{X}^n)$ where $Q(\mathbf{X}^n)Q(\mathbf{X}^n)^T = 2k_B T M(\mathbf{X}^n)/\Delta t$ with $\boldsymbol{\xi}$ a standard Gaussian random variate with independent components having mean zero and variance one. The thermal drift $k_B T \nabla \cdot \mathbf{M}$ is approximated by numerically estimating an average by $\langle Z\rangle_{\bar{N}} = 1/\bar{N}\sum_{k=1}^{\bar{N}} Z^{[k]}$. For the random variable Z, the $Z^{[k]}$ denotes one of the $\bar{N}$ independent samples. This probabilistic estimator provides an estimator for the divergence since for the random variables $\mathbf{p}$ and $\mathbf{q}$ satisfying $\langle p_i q_j\rangle = \delta_{ij}$ we have

(55)

$$\lim_{\delta \to 0} \delta^{-1}\left\langle\left(M\left(\mathbf{X} + \delta\mathbf{p}\right) - M(\mathbf{X})\right)\mathbf{q}\right\rangle = \nabla \cdot M.$$

This follows an approach advocated by [20] and the validity follows readily from Taylor expansion of M in $\mathbf{X}$ [31].

The stochastic Velocity-Verlet scheme in equation 54 can be viewed in stages as follows. The $\tilde{\mathbf{X}}^{n+1}$ gives the predictor part of the update of the configuration that is used to evaluate the force $\tilde{\mathbf{F}}^{n+1}$ and mobility $M(\tilde{\mathbf{X}}^{n+1})$. The $\mathbf{X}^{n+1}$ gives the corrector part for the update of the configuration which makes use of the predictor data and additional contributions from the thermal drift term.

3.2.1. Generating Stochastic Forces from the Mobility Tensor

During numerical time-step integration of the drift-diffusion dynamics by equation 54, we

must generate the stochastic driving term $\mathbf{h}^n = Q(\mathbf{X}^n)\boldsymbol{\xi}^n$. A common way to do this is to determine from the mobility the square-root factor Q satisfying $Q(\mathbf{X}^n)Q(\mathbf{X}^n)^T = 2k_BTM$. Cholesky factorization provides a convenient method for this for symmetric positive definite matrices [80]. However, in the current formulation this present challenges given that the mobility tensor for the surface hydrodynamics is singular since it only depends on the tangential component of the force, see equation 39. One may be tempted to work only with the surface coordinates. For the sphere, this presents challenges since there is no global coordinate chart for such topologies [75]. We have chosen instead to work in the embedding space resulting in a mobility tensor representation that is only positive semi-definite precluding the direct use of Cholesky factorization.

We remedy this situation by adding a block diagonal tensor to our grand mobility tensor of equation 36. We construct using rank-one stabilizations modified self-mobility tensor blocks $\tilde{M}_{ii} = M_{ii} + \alpha\mathbf{n}_i\mathbf{n}^T$, where α is any positive weight. The $\mathbf{n}_i$ denotes the normal vector on the sphere at the location of $\mathbf{X}_i$. With this modified mobility tensor, we can now use Cholesky factorization to obtain $\tilde{Q}$ satisfying $\tilde{Q}(\mathbf{X}^n)\tilde{Q}(\mathbf{X}^n)^T = 2k_BT\tilde{M}$.

This is useful since the stabilizations constructed are orthogonal to the tangent directions of the surface and would only effect mobility responses in the dynamics of the particles in the directions normal to the surface. As a consequence, we can generate the needed tangential stochastic forces using $\mathbf{h} = \wp\tilde{\mathbf{h}}^n$ where $\tilde{\mathbf{h}}^n = Q(\mathbf{X}^n)\boldsymbol{\xi}^n$ with $\boldsymbol{\xi}^n$ a Gaussian vector with independent components having mean zero and variance one. The $\wp$ here denotes projection of the stochastic driving vector $\tilde{\mathbf{h}}^n$ to the tangent space of the surface. In this manner, we obtain the needed stochastic terms to account for the thermal fluctuations in the drift-diffusion dynamics on the surface for the microstructures.

3.3. Computing Hydrodynamic Forces and Responses

To solve for the fluid velocity, we represent the force density term as $c = - \star \mathbf{db}^\flat$ with expansion $c = \sum_\ell c_s Y_s$. We compute this in practice by using the spherical harmonics representation of $\mathbf{b}$ obtained by $\hat{b}_s^{[a]} = \langle b^{[a]}, Y_s \rangle$ where the inner-product is approximated numerically by using Lebedev quadrature [49, 50]. The $\mathbf{b} = b^{[a]}\partial_{z^a}$ gives the representation of the force density $\mathbf{b}$ in the ambient physical space with coordinates z^a. We then compute $c = - \star \mathbf{db}^\flat = \sum_s(- \star \mathbf{d})\mathbf{b}_s$ using the finite spherical harmonics expansion of $\mathbf{b} = \sum_s \mathbf{b}_s$ with $\mathbf{b}_s$ denoting the term of the expansion associated with index s. We compute c_s using $c_s = \langle c, Y_s \rangle$ where the inner-product is approximated numerically using Lebedev quadrature [49, 50]. From the solution coefficients a_s, we obtain the fluid velocity on the surface from $\mathbf{v} = \sum_s a_s(- \star \mathbf{d}Y_s)^\sharp$.

In practice, we numerically approximate L^2 inner-products by using Lebedev quadratures on the spherical surface [49, 50, 75]. We use $\langle u, v \rangle = \langle u, v \rangle_Q = \sum w_i u(\mathbf{x}_i)v(\mathbf{x}_i)$, where $\langle u, v \rangle_Q$ denotes the quadrature computed inner-product with w_i the weights and $\mathbf{x}_i$ the nodes [49, 50, 75]. This provides a finite spherical harmonics expansion of $- \star \mathbf{db}$. While other quadrature approaches could be used such as lattitude and longitude sampling, the Lebedev quadrature nodes have octahedral symmetry and provide a better distribution of sampling nodes on the spherical surface [34, 75].

4. Applications

We discuss a few applications of our introduce fluctuating hydrodynamics computational methods for investigating phenomena within curved fluid interfaces. We first discuss the hydrodynamic relaxation of fluctuating fluids and characterize scalings of the velocity autocorrelation function. We find different scalings can emerge de-

pending on the physical regimes associated with the interface geometry, surface viscosity, and bulk viscosity. We further investigate the mobilities associated with microstructures embedded within fluid interfaces in the quasi-steady regime. We then demonstrate the computational methods by studying the correlated diffusion of passive particles and the drift-diffusion dynamics of active microswimmers. The results show some of the significant roles played by hydrodynamic coupling within curved fluid interfaces.

4.1. Autocorrelations of the Surface Fluctuating Hydrodynamics

We investigate the autocorrelation of the fluid velocity of interfacial fluctuating hydrodynamics introduced in equation 5. We find the velocity autocorrelations can exhibit power-law decay with scalings τ^{-1} and τ^{-2} depending on the physical regime. We also find in some regimes a plateu behavior can arise. This differs significantly from bulk fluctuating hydrodynamics that exhibits a characteristic $\tau^{-3/2}$ power-law decay [7,8].

Interfacial fluctuating hydrodynamics involves both dissipation from the propogation of shearing motions within the interfacial fluid surface and from traction coupling with the bulk surrounding fluid. This results in two important time-scales. The first is the time-scale for shear stresses to propogate over the entire spherical surface $\tau_f = R^2/\mu_m$. The second is the time-scale on which rigid-body rotation of the entire spherical interface dissipates energy significantly to the bulk surrounding fluid $\tau_r = RL/\mu_m$.

Surface Fluctuating Hydrodynamics: Velocity of Spontaneous Flows
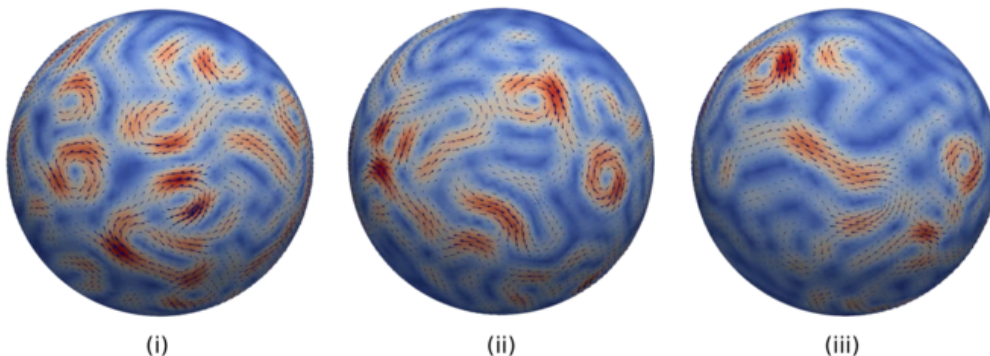

(i)　　　　　(ii)　　　　　(iii)

Figure 2: *Surface Fluctuating Hydrodynamics and Velocity of Spontaneous Flows. We show a few samples of the fluid velocity of the surface fluctuating hydrodynamics. We emphasize these results have an introduced correlation length-scale by use of a finite spherical harmonics expansion with modes up to degree $N = 20$. In the drift-diffusion dynamics of microstructures, similar correlations arise from the averaging operator Γ. The surface fluctuating hydrodynamics incorporates the dissipation from both the interfacial shear viscosity and the traction stresses with the inner and outer bulk surrounding fluids using equation 22. The incompressibility of the fluid and the spherical topology induces long-range correlated structures that manifest as recirculation patterns on the surface.*

We explore these contributions to the velocity autocorrelations by varying the ratio $\tau_f/\tau_r = R/L$ involving the sphere radius R to the Saffman-Delbrück length L. We show our results in Figure 3. We take as default parameter values $\rho = 1$, $\mu_m = 1$, $K_B T = 1$, $R = 1$, $L = 1$, and $\ell \leq N = \ell_* = 50$. We give details on our derivations analyzing these autocorrelations in

Appendix B.

The velocity autocorrelations of the surface fluctuating hydrodynamics can be expressed using an expansion in spherical harmonics as

$$\left\langle v^\phi(0)v^\phi(t)\right\rangle \qquad (56)$$

$$= \sum_s \exp(tL_s)\frac{k_BT}{|g|\rho\ell(\ell+1)}\left|\frac{\partial Y_s}{\partial\theta}\right|^2$$

$$\approx C\frac{k_BT}{|g|\rho}\sum_\ell\left(\ell+\frac{1}{2}\right)\exp(tL_\ell).$$

The v^ϕ denotes the ϕ-directional component of the velocity, the Y_s denotes the spherical harmonic with mode $s=(\ell,m)$, the metric factor on the sphere is $|g|=R^2$. We also use that the velocity is isotropic and that $\langle a_s^2\rangle = k_BTR^2/\rho\ell(\ell+1)$ and $\langle a_s(0)a_s(t)\rangle = \langle a_s^2\rangle\exp(tL_s)$, where L_s is given in equation 43. We derive scaling laws for different physical regimes using equation 56. We remark that all of our results use a truncated expansion with modes up to degree $N=50$. This introduces a regularization length-scale similar to our immersed boundary coupling approaches for determining responses of particles and microstructures. Details of our derivations can be found in Appendix B.

When $R/L \ll 1$, we find the velocity correlations exhibit an initial decay to a power-law regime with scaling τ^{-1} on time-scales $\tau \ll \tau_f$. This is followed by a plateau regime that persists from $\tau_f \ll \tau \ll \tau_r$. This eventually gives way to exponential decay for $\tau \gg \tau_r$. The initial τ^{-1} power law decay is associated with the propogation of shear stresses over the interface with negligible dissipation to the bulk. This persists until time-scale τ_f, see Figure 3.

A plateau arises in the case when $\tau_r \gg \tau_f$ where there is an intermediate regime that exists. In the intermediate plateau regime the shear stress has already propagated to the entire surface, but the dissipation into the bulk fluid of the rigid-body rotational motion has not yet become significant. On time-scales $\tau \gg \tau_r$, dissipation

into the bulk fluid dominates through the rotational motions and gives exponential decay. As the R/L increases, the plateau regime disappears when $\tau_r \sim \tau_f$, as seen when moving left to right in Figure 3.
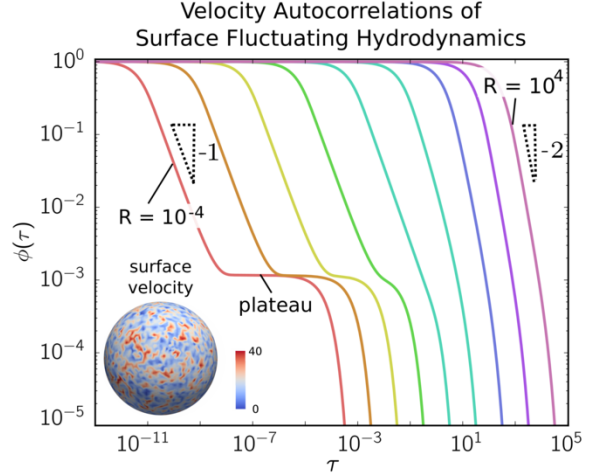

Figure 3: *Velocity Autocorrelations of Surface Fluctuating Hydrodynamics. For the interfacial fluctuating hydrodynamics introduced in equation 5 we show the temporal autocorrelation $\phi(\tau) = \langle\mathbf{v}(0)\cdot\mathbf{v}(t)\rangle/\langle\mathbf{v}^2(0)\rangle$. The curves left to right have $R=10^\alpha$ with integer values in range $\alpha \in [-4,4]$. We see the velocity autocorrelation exhibits regimes with power-law decay τ^β with $\beta = -1,-2$ (dotted lines) and plateaus. The surface fluctuating hydrodynamics where sampled with truncated expansion with modes up to degree $N=50$. We derive these power-laws for surface fluctuating hydrodynamics in Appendix B.*

In the $R/L \gg 1$ regime, the time-scales for decay from intra-interface shearing motions becomes reversed and large relative to the time-scale for decay from the coupling to the bulk fluid $\tau_f \gg \tau_r$. This results in a new regime with power law scaling τ^{-2} for time-scales $\tau \ll \tau_r$. When $\tau \gg \tau_f$ this gives way again to exponential decay from the rotational motions of the entire interface. The τ^{-2} arises from simultaneous dissipation from the shearing motions within the interface and dissipation from coupling to the bulk fluid. We give more details and derivations

of these power-laws and related time-scales in Appendix B.

Mobility $M_{\|\|\|}$

Figure 4: *Mobility Response* $\mathbf{V}_\| = M_{\|\|\|}F_\|$. *We show the mobility response component when a unit force is applied to the first particle in the direction parallel to the separation of the two particles. We scale the mobility by $M_0 = 641$ corresponding to a pure rotational response. The response* $\mathbf{V}_\perp = M_{\perp\|\|}F_\|$ *was found to be negligble with a magnitude smaller than 0.01% of M_0.*

4.2. Mobility Tensor for Interacting Particles and Microstructures

We compute numerically the mobility of equation 36 as $\tilde{M}(\mathbf{X}) = \Gamma\tilde{\mathcal{S}}\Lambda$. We obtain a numerical solver $\tilde{\mathcal{S}}$ for the fluid velocity $\tilde{\mathbf{v}}^\flat = \tilde{\mathcal{S}}\Lambda[\mathbf{F}]$ with force distribution $\mathbf{f}^\flat(\mathbf{x}) = \Lambda[\mathbf{F}](\mathbf{x})$ on the spherical surface using equation 40 and Lebedev quadratures [49, 50, 75].

From the symmetry of the sphere the mobility of N particles can be determined from the canonical two particle mobility tensor. The two particle mobility obtained from equation 36 can be expressed as

$$M = \left[\begin{array}{cc} M_{11} & M_{12} \\ M_{21} & M_{22} \end{array} \right] \qquad (57)$$

with

$$\bar{M}_{12} = \left[\begin{array}{cc} M_{\|\|\|} & M_{\|\perp} \\ M_{\perp\|} & M_{\perp\perp} \end{array} \right]. \qquad (58)$$

The $M_{ij} = \Gamma_i\tilde{\mathcal{S}}\Lambda_j$ where we use notation $\Gamma_i\mathbf{v}^\flat = \Gamma[\mathbf{X}_i]\mathbf{v}^\flat$ and $\Lambda_j[\mathbf{F}](\mathbf{x}) = \Lambda[\mathbf{X}_j][\mathbf{F}](\mathbf{x})$. The M_{ii} denote the self-mobilities and can be computed numerically once and stored.
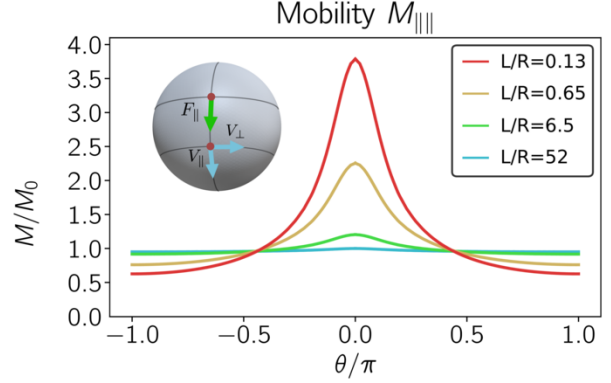
The $\bar{M}_{12}$ give for a force $\mathbf{F}$ on the first particle the velocity response $\mathbf{V}$ at the second particle. We can express this as $\mathbf{V} = V_\|\mathbf{e}_\| + V_\perp\mathbf{e}_\perp$, where for the two particle displacement we split into the parallel $\|$ and perpendicular $\perp$ components. The $V_\| = M_{\|\|\|}\mathbf{F}_\| + M_{\|\perp}\mathbf{F}_\perp$ and $V_\perp = M_{\perp\|}\mathbf{F}_\| + M_{\perp\perp}\mathbf{F}_\perp$. Using the symmetry of the sphere we can tabulate numerically the two particle mobility tensor by using a canonical configuration of the two particles. We rotate the sphere so that the first particle is always situated at the north pole. We then align the geodesic displacement between the two particles in the xz-plane with tangent along the positive x-axis. We denote the rotation operation by $\mathcal{R}^T$ that moves any two particles into this canonical configuration $\tilde{\mathbf{X}} = \mathcal{R}^T\mathbf{X}$. We can convert our canonical tabulated two-particle mobilities to the specific mobility of two particles by $M_{12} = \mathcal{R}\tilde{M}_{12}\mathcal{R}^T$. We obtain the grand-mobility tensor M for n interacting particles by summing over all pairs of particles the two particle mobility tensors. We show the components of the two-particle mobility $\bar{M}_{12}$ when $L/R = 0.13, 0.65, 6.5, 52$ in Figure 4
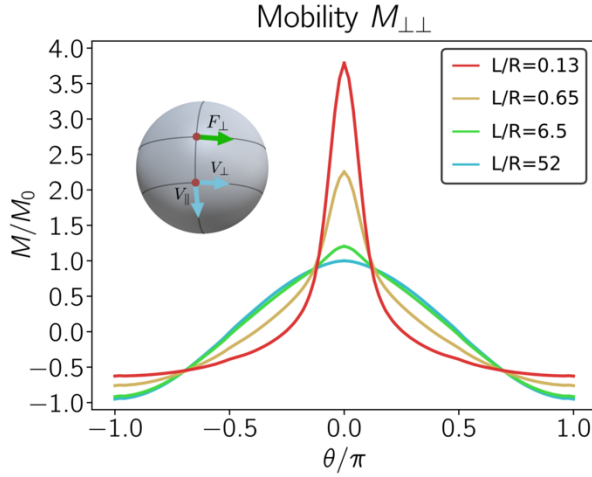
and [5].

Figure 5: *Mobility Response* $\mathbf{V}_\perp = M_{\perp\perp} F_\perp$. *We show the mobility response component when a unit force is applied to the first particle in the direction perpendicular to the separation of the two particles. We scale the mobility by $M_0 = 641$ corresponding to a pure rotational response. The response $\mathbf{V}_\parallel = M_{\parallel\perp} F_\perp$ was found to be negligble with a magnitude smaller than 0.01% of M_0.*

4.3. Equilibrium Fluctuations

We validate our stochastic numerical methods by studying the drift-diffusion dynamics of interacting particles. A strong indication of the validity the methods is provided by consider how particles diffuse over time when subject to a conservative force. This requires the stochastic methods to capture both the drift dynamics accurately while also handling appropriately the thermal fluctuations of the system. From equilibrium statistical mechanics a configuration should have a probability distribution $\rho(\mathbf{X})$ of the Gibbs-Boltzmann form [17,71]

$$\rho(\mathbf{X}) = \frac{1}{Z} \exp\left[-\phi(\mathbf{X})/k_B T\right]. \qquad (59)$$

The Z denotes the partition function and $k_B T$ denotes the thermal energy of the system [71].
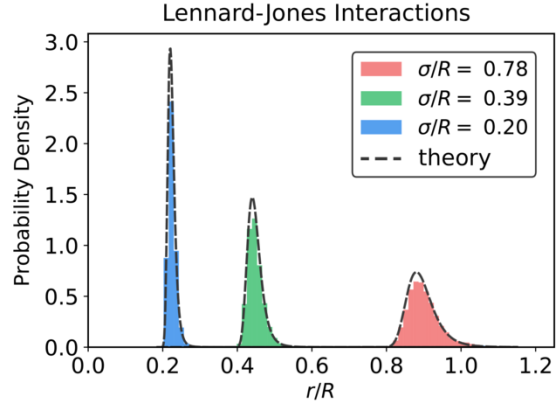

Figure 6: *Gibbs-Boltzmann Distribution. We compute using our stochastic numerical methods of equation [54] the equilibrium fluctuations associated with the drift-diffusion motions of hydrodynamically coupled particles having Lennard-Jones interactions of equation [60]. We test interactions for a few choices of σ and find good agreeement between our numerical results and the Gibbs-Boltzmann distribution predicted by equation [59].*

We consider the drift-diffusion dynamics of two hydrodynamically coupled particles having the non-linear Lennard-Jones interaction

$$\phi(r) = 4\epsilon \left(\left(\frac{\sigma}{r}\right)^{12} - \left(\frac{\sigma}{r}\right)^6 \right). \qquad (60)$$

The r denotes the distance between the two particles. The σ denotes the length-scale characteristizing the radius of the particles. We find our stochastic numerical methods provide for the drift-diffusion dynamics very good agreement with the distribution predicted from equilibrium statistics mechanics from equation [59]. We show these results for a few choices of σ in Figure [6].

For parameters, we take throughout the thermal energy $k_B T = 2.48\,\text{amu·nm}^2/\text{ps}^2$, the strength of the potential $\epsilon = 10 K_B T$, viscosity ratio $L/R = 0.65$. We use for the stochastic integrator in equation [54] the time-steps $\Delta t = 1.3 \times 10^5$ ps and drift estimator $\delta = 10^{-1}$, $\bar{N} = 10$.

4.4. Hydrodynamic Correlations in Particle Diffusion

Motivated by proteins in lipid bilayer membranes and recent results for synthetic colloidal systems [16, 19, 29, 58], we consider diffusion limited interactions by particles that interact within a curved fluid interface. We investigate the case with and without hydrodynamic coupling on the collective diffusivity and how this influences the time for particles to come into near contact.
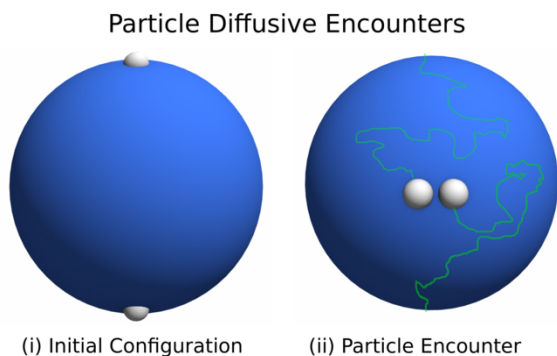

Particle Diffusive Encounters

(i) Initial Configuration   (ii) Particle Encounter

Figure 7: *Diffusive Encounters between Two Particles. We show a schematic of our study of the distribution of times for two diffusing particles to come into contact. The two particles start respectively at the north and south poles (left). In the cases with and without hydrodynamic coupling, we investigate the distribution of times for when the particles come into diffusive contact (right).*

We consider two particles initially at anti-podal locations on the sphere (north and south pole) and the amount of time it takes for them to come into contact with each other. We consider the distribution for this meeting time in the case of hydrodynamic coupling with mobility M as in Section 4.1 and in the case without hydrodynamics with a local drag having mobility response $M = -\gamma\mathcal{I}$. We report these results with and without hydrodynamic interactions in Figure 8. We use in our studies the parameter values in Table 1.

Parameter	Value	Parameter	Value
R	15.3nm	$R_{particle}$	1.5nm
$k_B T$	2.48u nm^2 ps^{-1}	D	3e-7nm^2 ps^{-1}
γ_{drag}^{-1}	$D/k_B T$	γ_{slip}	0.15
τ_D	R^2/D	Δt	5e-6τ_D
L^+	100		

Table 1: *Parameters used for the pair diffusivity study and simulations. We use SI units of atomic-mass-units (u), nanometers (nm), and picoseconds (ps).*

We find in both cases that the meeting times remain on average on the same order of magnitude. However, the hydrodynamic coupling introduces significantly more variation in the meeting-time distribution producing a long-tail, see Figure 8. For systems where diffusive kinetics are important, we see the hydrodynamic coupling can significantly influence the distribution of encounters between particles.
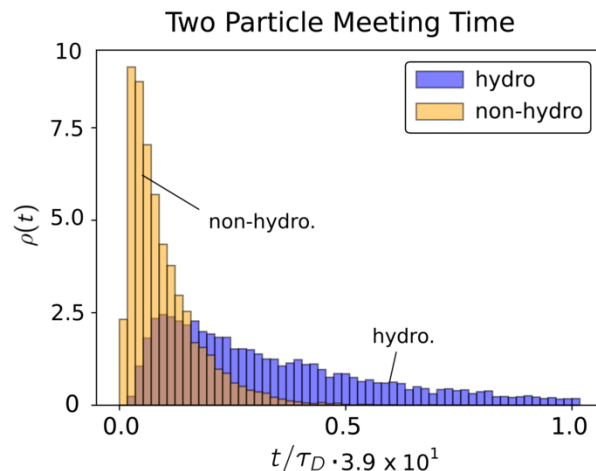

Figure 8: *Two Particle Pair-Meeting Time Distribution. For two particles starting at antipodal locations on the sphere, we show the distribution of times for the two particles to come into contact at critical distance $r \leq \tilde{r}_c = 3R_{particle}$.*

4.5. Microscopic Swimmers and Mixing

We investigate hydrodynamic transport and diffusive mixing associated with swimmers at microscopic scales. Behaviors both individually and col-

lectively can differ significantly from macroscopic scales [48,68]. Swimming in both Newtonian and Non-Newtonian bulk fluids in three dimensional volumes have been investigated in [48,59,68]. We investigate here the case of swimmers within two dimensional curved fluid interfaces treated as a Newtonian fluid. Our approaches also could be used to study non-Newtonian fluids either by incorporating explicitly the microstructures in the fluid using approaches of Section 2.5 and [10], or by extending the formulation of the hydrodynamic equations to other constitutive laws in Section 2.1.

As a demonstration of the methods, we consider Golestanian Swimmers [59] that consist of three beads that interact through two oscillating harmonic bonds. The harmonic bonds have time-dependent rest-lengths with energy

$$E_i(r) = \frac{1}{2}k[r - (l + A\sin(\omega t + \phi_i))]^2, \quad (61)$$

where $i = 0, 2$. The bond lengths are offset in time to have different phases for ϕ_0 and ϕ_2. To impose excluded volume, both the beads of the microscopic swimmers and the passive particles also interact through the Weeks-Chandler-Andersen (WCA) potential [84]

$$U_{\text{wca}}(r) = \begin{cases} 4\epsilon_{wca}\left[\left(\dfrac{\sigma_{wca}}{r}\right)^{12} \right. \\ \left. \qquad - \left(\dfrac{\sigma_{wca}}{r}\right)^6\right], & r \leq 2^{1/6}\sigma_{wca} \\ -\epsilon_{\text{wca}}, & r > 2^{1/6}\sigma_{wca}. \end{cases}$$

$$(62)$$

The separation distance is denoted by $r = \|\mathbf{X}_i - \mathbf{X}_j\|$ for two particles $\mathbf{X}_i$ and $\mathbf{X}_j$. The potential gives an effective particle steric radius of $r_s = 2^{1/6}\sigma_{wca}$. We give parameters for our model in Table 2. We remark that this parameterization is for illustrative purposes of the methods and to obtain more physically realizable systems may require further adjustments.

Variables	Values		Variables	Values
R	15.3nm		$R_{particle}$	1.5nm
k_BT	2.48unm^2/ps^2		D	9.4577e-1nm^2 ps^{-1}
τ_D	R^2/D		Δt	5e-7τ_D
t	5e5Δt		γ_{slip}	2.6222e-3 ps u^{-1}
resI	100		γI	800
N	3 particles		k	5e2k_BT
ϵ_{wca}	5k_BT		σ_{wca}	2$R_{particle}$
ϕ_0	0		ϕ_2	$\pi/2$
A	$R_{particle}$		l	2$R_{particle}$
ω	5e-3			

Table 2: *Parameter Values for the Swimmer Simulations. We use SI units of atomic-mass-units (u), nanometers (nm), and picoseconds (ps).*

The phase differences in the swimming strokes are crucial to break symmetry in time for the possibility of net forward motion. For steady-state hydrodynamics, a time-reversable motion would have no net displacement by the Scallop Theorem [42,47,68]. We also emphasize that without hydrodynamic coupling between the beads the swimmer would remain stationary. This is a consequence of the equal-and-opposite forces that act on the beads and average out to zero over the periodic strokes. Without the surrounding fluid, such forces can not move the center-of-mass of the swimmer.

Golestanian Swimmer Stroke Cycle in the Spherical Fluid Interface
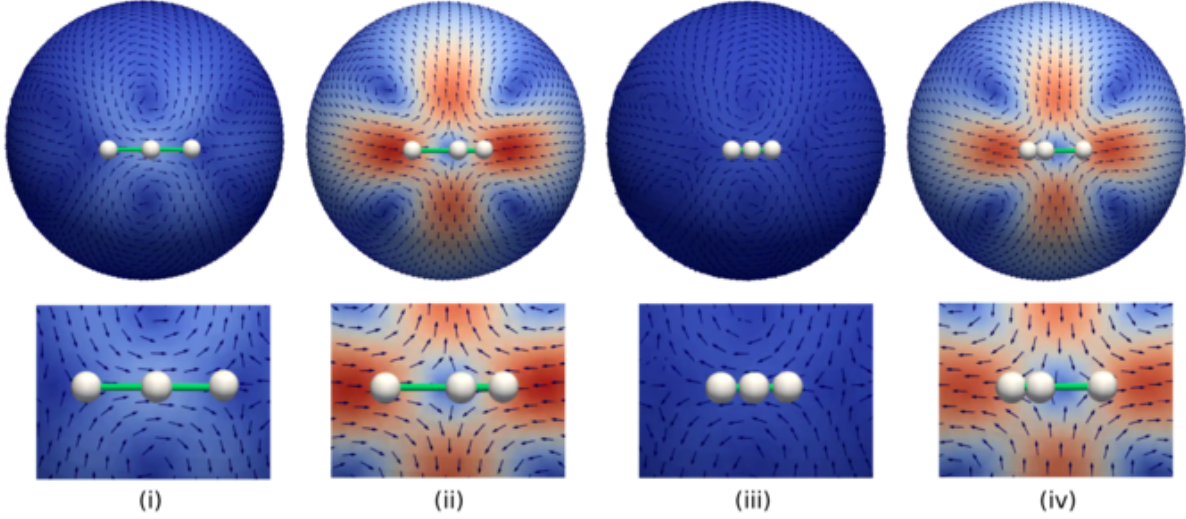
(i)   (ii)   (iii)   (iv)

Figure 9: *Stroke Cycle and Hydrodynamic Flows of the Golestanian Microswimmer. For the three bead Golestanian swimmer [59] immersed within a spherical fluid interface, we show the configurations at each stage during the swimming cycle and associated hydrodynamic flow for $L/R = 6.5$. Different flows are generated when the beads of the microswimmer are pushing or pulling with respect to one another within the fluid. The motions are by design non-reversable in time and result in the microswimmer having net forward motion to the right. We show the average flow generated in the inset of Figure 10.*

The swimmer strokes generate flows that on average pump the fluid. We show the associated stages of the stroke cycle captured by our methods in Figure 9. The hydrodynamics is confined to a surface of spherical topology which results in flows with vortices. We show the average flow that pumps the fluid in the inset of Figure 10.

We study first how the swimmer's speed depends on the viscosities of the two dimensional interfacial fluid and surrounding bulk fluid. We characterize the viscosities by the ratio L/R of the Saffman-Delbrück length L to the sphere radius R as discussed in Section 2.7. We can consider the swimmer's angular progression over the sphere from which the swimming speed can be estimated, see Figure 10. As the viscosity ratio L/R increases, the generated flows transition from being relatively localized to enveloping most of the sphere. We find as the viscosity ratio increases from $L/R = 0.13$ to $L/R = 52$ that the

swimming speed drops by approximately $\sim 25\%$, see Table 3.

We next investigate the collective drift-diffusion dynamics of N_T passive particles when subjected to mixing by multiple microscopic swimmers N_S. Both the swimmers and particles are subjected to the hydrodynamic coupling and thermal fluctuations using the approaches we introduced in Section 2. We study as the number of microscopic swimmers increases how the effective diffusivity of the passive tracer particles is influenced.

We characterize the diffusivity by the Mean Squared Displacement (MSD)

$$MSD(t) = \left\langle \|X(t) - X(0)\|_g^2 \right\rangle. \tag{63}$$

In the spherical geometry the standard Euclidean distance is distorted by the spherical surface. We use as our norm $\| \cdot \|_g$ the geodesic distance on the surface between the starting point $X(0)$ and

the final point $X(t)$. Unlike bulk three dimensional fluids, the distance between points remains bounded since the surface is a compact manifold. As a consequence, we have that eventually the $MSD(t) \to m_0^2$ asymptotes to a limiting value. This corresponds to sampling the $X(t)$ from the stationary distribution over the surface.

To estimate in practice the diffusivity, we consider the MSD over time-scales τ with $\tau \leq 0.06\tau_D$ where τ_D is the time-scale to diffuse the distance R. We find the MSD is approximately linear in this regime and we characterize the passive particle motions by the diffusivity $D = \partial MSD(t)/\partial t$, see Figure 12. In practice, we estimate D using the slope of the MSD obtained from a least-squares fit to the data in the range $0 \leq t \leq 0.06\tau_D$.
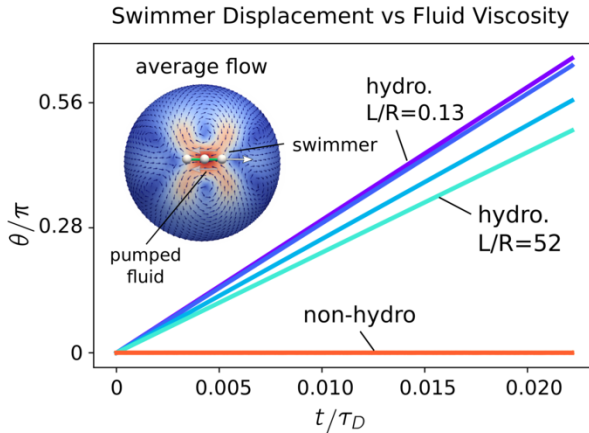

Figure 10: *Swimming Velocity on the Spherical Fluid Interface when varying the Fluid Viscosities. We show how the angular velocity and associated displacement of microswimmers vary as the viscosity ratio L/R increases. We find the swimmer speed reduces over the viscosity range by $\sim 25\%$, see Table 2. We also show the results for the swimmer when neglecting hydrodynamic coupling which as expected does not result in any significant forward motion. We show the time-averaged hydrodynamic flow generated by the swimmer for $L/R = 6.5$ in the inset.*

L/R	v/v_0 (hydro)	L/R	v/v_0 (hydro)
0.13	1.167330	6.5	1.000000
0.65	1.138532	52	0.881074

Table 3: *Estimated swimmer velocity from the simulated swimmer displacements with and without hydrodynamic coupling in Figure 10. Velocities normalized by $v_0 = 4.55 \times 10^3$nm/ps when $L/R = 6.5$. The non-hydrodynamic swimmer simulations did not exhibit any significant net motions $v/v_0 \sim 5.93 \times 10^{-4}$nm/ps. We remark that this parameterization in Table 3 is for illustrative purposes of the methods and to obtain more physically realizable systems may require further adjustments.*

We study how the diffusivity D of $N_T = 80$ passive tracer particles are enhanced by the action of N_S swimmers. Both the passive tracers and swimmers undergo the drift-diffusive dynamics of equation 34 with parameters in Table 2. We remark there are some technical challenges in parameterizing consistently for comparisons the non-hydrodynamic and hydrodynamic dynamics. We choose to do this by using the diagonal entry of our mobility tensor $M_{\parallel\parallel}$ as the inverse drag γ_{drag}^{-1} for the non-hydrodynamic dynamics. Given symmetries that can arise readily for small numbers of swimmers, we consider cases with $N_S \in [5, 10]$.

Our initial studies reported here find the swimmers can result in significant enhancement of the tracer diffusivity relative to the non-hydrodynamic case, see Figure 12. In the case with no swimmers $N_S = 0$, we have diffusivity with hydrodynamic coupling $D_{hy} = 1.70295$nm^2/ps and without hydrodynamic coupling $D_{nh} = 1.3916$nm^2/ps. This has the ratio $D_{hy}/D_{nh} = 1.2237$. We see already in the absence of any swimmers an effective enhancement of $\sim 20\%$ in the diffusivity of the particles from the hydrodynamic correlations.
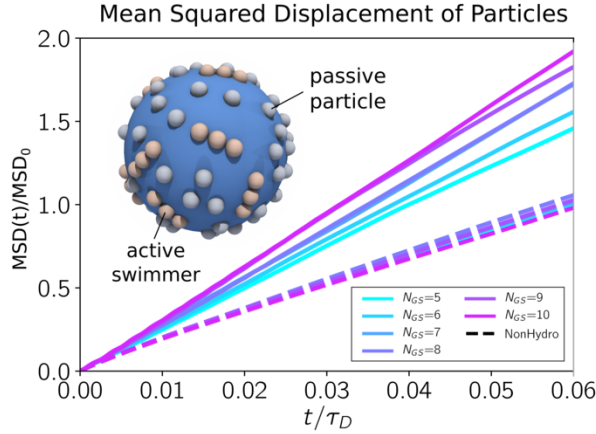
Figure 11: *Mean Squared Displacement (MSD) for Different Number of Swimmers. We show over time t the $MSD(t)$ from equation 63. We see the hydrodynamic flows generated by the swimmers can significantly enhance the MSD. In contrast, in the absence of hydrodynamic coupling the MSD of the tracer particles changes relatively little. The MSD is normalized by $MSD_0 = MSD(t^*) = 0.1762\text{nm}^2$ at time $t^* = 0.06$ for $N_S = 5$ without hydrodynamics. We show in the inset a typical configuration of the swimmers and tracer particles for $N_T = 80$ and $N_S = 10$.*

As we introduce microscopic swimmers that have stroke cycles that generate hydrodynamic flows in addition to the thermal fluctuations, and increase N_S, we find the diffusivity is further enhanced relative to the non-hydrodynamic case from approximately $\sim 40\%$ to $\sim 100\%$, see Figure 12. The thermal fluctuations allow for the tracer particles to diffuse between streamlines of the hydrodynamic flows that are transiently generated by the swimmers. The swimmers also can have their own motions driven by the mutual flows and thermal fluctuations that serve both to move their center-of-mass and to rotate their orientation. This combination of effects shows the interplay that can arise between hydrodynamically driven drifts and thermal fluctuations.

The results illustrate some of the hydrodynamics effects that can be captured by our methods that also could be particularly important in processes arising in other systems with rich mi-

crostructures, such as passive and active soft materials [55] or in cell mechanics in biology [13, 57]. The introduced fluctuating hydrodynamics methods can be applied quite generally to passive and active spatially extended microstructures to capture both the hydrodynamic coupling and the correlated thermal fluctuations within fluid interfaces.
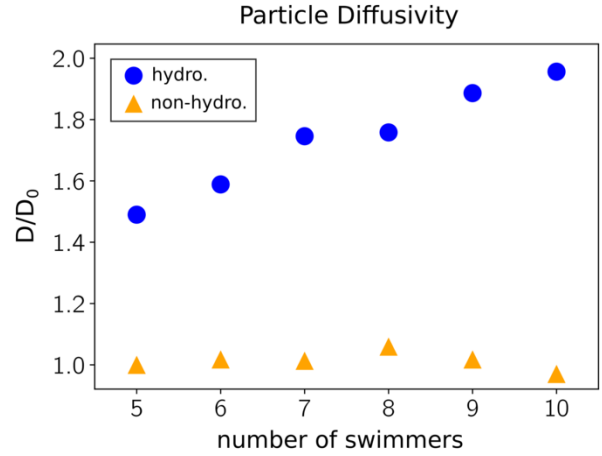

Figure 12: *Diffusivity verses Number of Swimmers. We show how the enhanced diffusivity depends on the number of microscopic swimmers. We see that as the number of swimmers increases the diffusivity is significantly enhanced from $\sim 40\%$ to almost $\sim 100\%$ relative to the case without hydrodynamic coupling where diffusivity remains constant. The results are normalized by $D_0 = 1.3703\text{nm}^2/\text{ps}$ for the diffusivity in the case without hydrodynamic coupling and $N_S = 5$ swimmers.*

5. Conclusions

We have introduced general fluctuating hydrodynamics approaches for investigating the drift-diffusion dynamics of particles and microstructures immersed within curved fluid interfaces. We introduced general computational methods for capturing fluid-structure interactions and collective dynamics driven by thermal fluctuations and active forces. We have used these approaches to investigate general phenomena associated with

the autocorrelations of fluctuating hydrodynamics of interfaces finding there are different scalings that emerge in physical regimes depending on the interface geometry, surface viscosity, and bulk viscosities. We demonstrated how our methods can be used in practice to to investigate the collective diffusion of particles and microstructures. The results show some of the rich phenomena that can arise for curved fluid interfaces that can be captured by the introduced surface fluctuating hydrodynamics methods.

6. Acknowledgments

References

[1] R. Abraham, J.E. Marsden, and T.S. Raiu. *Manifolds, Tensor Analysis, and Applications.* Number v. 75. Springer New York, 1988.

[2] B. Alberts, A. Johnson, P. Walter, J. Lewis, M. Raff, and K. Roberts. *Molecular Cell Biology of the Cell, 5th Ed.* Garland Publishing Inc, New York, 2007.

[3] B. J. Alder and T. E. Wainwright. Decay of the velocity autocorrelation function. *Phys. Rev. A*, 1(1):18–21, January 1970.

[4] Tadashi Ando and Jeffrey Skolnick. Crowding and hydrodynamic interactions likely dominate in vivo macromolecular motion. *Proceedings of the National Academy of Sciences*, 107(43):18457–18462, 2010.

[5] Marino Arroyo and Antonio DeSimone. Relaxation dynamics of fluid membranes. *Phys. Rev. E*, 79(3):031915–, March 2009.

[6] Kendall Atkinson and Weimin Han. *Spherical Harmonics and Approximations on the Unit Sphere: An Introduction.* Springer, 2010.

[7] P. J. Atzberger. Velocity correlations of a thermally fluctuating brownian particle: A novel model of the hydrodynamic coupling. *Physics Letters A*, 351(4-5):225–230–, 2006.

[8] P. J. Atzberger, P. R. Kramer, and C. S. Peskin. A stochastic immersed boundary method for fluid-structure dynamics at microscopic length scales. *Journal of Computational Physics*, 224(2):1255–1292–, 2007.

[9] Paul J. Atzberger. Stochastic eulerian lagrangian methods for fluidstructure interactions with thermal fluctuations. *Journal of Computational Physics*, 230(8):2821–2837, April 2011.

[10] Paul J. Atzberger. Incorporating shear into stochastic eulerian-lagrangian methods for rheological studies of complex fluids and soft materials. *Physica D: Nonlinear Phenomena*, 265:57 – 70, 2013.

[11] P.J. Atzberger. Spatially adaptive stochastic numerical methods for intrinsic fluctuations in reaction-diffusion systems. *Journal of Computational Physics*, 229:3474–3501, 2010.

[12] D. Bedeaux and P. Mazur. Brownian motion and fluctuating hydrodynamics. *Physica*, 76(2):247–258, September 1974.

[13] D. Boal. *Mechanics of the Cell*. Cambridge University Press, Cambridge, UK, 2002.

[14] F Bresme and M Oettel. Nanoparticles at fluid interfaces. *Journal of Physics: Condensed Matter*, 19(41):413101, 2007.

[15] Brian A. Camley and Frank L. H. Brown. Fluctuating hydrodynamics of multicomponent membranes with embedded proteins. *The Journal of Chemical Physics*, 141(7):075103, 2014.

[16] Marcello Cavallaro, Lorenzo Botto, Eric P. Lewandowski, Marisa Wang, and Kathleen J. Stebe. Curvature-driven capillary migration and assembly of rod-like particles. *Proceedings of the National Academy of Sciences*, 108(52):20923–20928, 2011.

[17] D. Chandler. *Introduction to Modern Statistical Mechanics.* Oxford, New York, 1987.

[18] S.Q. Choi, S. Steltenkamp, J.A. Zasadzinski, and T.M. Squires. Active microrheology and simultaneous visualization of sheared phospholipid monolayers. *Nat Commun*, 2:312–, May 2011.

[19] S Dasgupta, T Auth, and G Gompper. Nano- and microparticles at fluid and biological interfaces. *Journal of Physics: Condensed Matter*, 29(37):373003, 2017.

[20] Steven Delong, Yifei Sun, Boyce E. Griffith, Eric Vanden-Eijnden, and Aleksandar Donev. Multiscale temporal integrators for fluctuating hydrodynamics. *Phys. Rev. E*, 90(6):063312–, December 2014.

[21] V. Démery and D. S. Dean. Drag forces on inclusions in classical fields with dissipative dynamics. *The European Physical Journal E*, 32(4):377–390, Aug 2010.

[22] Yegor A. Domanov, Sophie Aimon, Gilman E. S. Toombes, Marianne Renner, Francois Quemeneur, Antoine Triller, Matthew S. Turner, and Patricia Bassereau. Mobility in geometrically confined membranes. *Proceedings of the National Academy of Sciences*, 108(31):12605–12610, August 2011.

[23] J. R. Dorfman and E. G. D. Cohen. Velocity-correlation functions in two and three dimensions: Low density. *Phys. Rev. A*, 6(2):776–790, August 1972.

[24] Z. C. Feng and L. G. Leal. Nonlinear bubble dynamics. *Annual Review of Fluid Mechanics*, 29(1):201–243, 1997.

[25] Marshall Fixman. Simulation of polymer dynamics. i. general theory. *The Journal of Chemical Physics*, 69(4):1527–1537, 1978.

[26] Thomas Franosch, Matthias Grimm, Maxim Belushkin, Flavio M. Mor, Giuseppe Foffi, Lasz Forra, and Sylvia Jeney. Resonances arising from hydrodynamic memory in brownian motion. *Nature*, 478:85, October 2011.

[27] Daan Frenkel and Berend Smit. Chapter 4 - molecular dynamics simulations. In Daan Frenkel and Berend Smit, editors, *Understanding Molecular Simulation (Second Edition)*, pages 63–107. Academic Press, San Diego, 2002.

[28] Gerald G. Fuller and Jan Vermant. Complex fluid-fluid interfaces: Rheology and structure. *Annual Review of Chemical and Biomolecular Engineering*, 3(1):519–543, 2012. PMID: 22541047.

[29] Y. Gambin, R. Lopez-Esparza, M. Reffay, E. Sierecki, N. S. Gov, M. Genest, R. S. Hodges, and W. Urbach. Lateral mobility of proteins in liquid membranes revisited. *Proceedings of the National Academy of Sciences*, 103(7):2098–2102, 2006.

[30] C. W. Gardiner. *Handbook of stochastic methods.* Series in Synergetics. Springer, 1985.

[31] Richard R. Goldberg. *Methods of Real Analysis.* Hamilton Printing Company, 2 edition, 1976.

[32] Melville S. Green. Markoff random processes and the statistical mechanics of time dependent phenomena. ii. irreversible processes in fluids. *The Journal of Chemical Physics*, 22(3):398–413, March 1954.

[33] B. Gross and P. J. Atzberger. Spectral numerical exterior calculus methods for differential equations on radial manifolds. *Journal of Scientific Computing*, Dec 2017.

[34] B. J. Gross and P. J. Atzberger. Hydrodynamic flows on curved surfaces: Spectral numerical methods for radial manifold shapes. 371:663–689, 2018.

[35] B. J. Gross, N. Trask, P. Kuberry, and P. J. Atzberger. Meshfree methods on manifolds for hydrodynamic flows on curved surfaces: A generalized moving least-squares (gmls) approach. *arXiv*, 2019.

[36] J. Happel and H. Brenner. *Low Reynolds Number Hydrodynamics: With Special Applications to Particulate Media.* Springer Netherlands, 1983.

[37] J. H. Heinbockel. *Introduction to Tensor Calculus and Continuum Mechanics.* Trafford, 2001.

[38] Mark L. Henle and Alex J. Levine. Hydrodynamics in curved membranes: The effect of geometry on particulate mobility. *Phys. Rev. E*, 81(1):011905–, January 2010.

[39] Eline Hermans, M. Saad Bhamla, Peter Kao, Gerald G. Fuller, and Jan Vermant. Lung surfactants and different contributions to thin film stability. *Soft Matter*, 11:8048–8057, 2015.

[40] Aurelia R. Honerkamp-Smith, Francis G. Woodhouse, Vasily Kantsler, and Raymond E. Goldstein. Membrane viscosity determined from shear-driven flow in giant vesicles. *Phys. Rev. Lett.*, 111(3):038103–, July 2013.

[41] Aurelia R. Honerkamp-Smith, Francis G. Woodhouse, Vasily Kantsler, and Raymond E. Goldstein. Membrane viscosity determined from shear-driven flow in giant vesicles. *Phys. Rev. Lett.*, 111(3):038103–, July 2013.

[42] Kenta Ishimoto and Michio Yamada. A coordinate-based proof of the scallop theorem. *SIAM Journal on Applied Mathematics*, 72(5):1686–1694, 2012.

[43] H. Kellay. Hydrodynamics experiments with soap films and soap bubbles: A short review of recent experiments. *Physics of Fluids*, 29(11):111113, 2017.

[44] U Kornek, F Mauller, K Harth, A Hahn, S Ganesan, L Tobiska, and R Stannarius. Oscillations of soap bubbles. *New Journal of Physics*, 12(7):073031, 2010.

[45] Ryogo Kubo. Statistical-mechanical theory of irreversible processes. i. general theory and simple applications to magnetic and conduction problems. *J. Phys. Soc. Jpn.*, 12(6):570–586, June 1957.

[46] H. Lamb. *Hydrodynamics.* University Press, 1895.

[47] Eric Lauga. Life around the scallop theorem. *Soft Matter*, 7:3060–3065, 2011.

[48] Eric Lauga and Thomas R Powers. The hydrodynamics of swimming microorganisms. *Reports on Progress in Physics*, 72(9):096601, 2009.

[49] V. I. Lebedev and D. N. Laikov. A quadrature formula for the sphere of the 131st algebraic order of accuracy. *Dokl. Math.*, 59(2):477–481, 1999.

[50] V.I. Lebedev. Quadratures on a sphere. *USSR Computational Mathematics and Mathematical Physics*, 16(2):10–24, 1976.

[51] Mina Lee, Ming Xia, and Bum Park. Transition behaviors of configurations of colloidal particles at a curved oil-water interface. *Materials*, 9(3):138, 2016.

[52] Alex J. Levine, T. B. Liverpool, and F. C. MacKintosh. Mobility of extended bodies in viscous films and membranes. *Phys. Rev. E*, 69:021503, Feb 2004.

[53] E.H. Lieb and M. Loss. *Analysis*. American Mathematical Society, 2001.

[54] Harishankar Manikantan and Todd M. Squires. Pressure-dependent surface viscosity and its surprising consequences in interfacial lubrication flows. *Phys. Rev. Fluids*, 2:023301, Feb 2017.

[55] M. C. Marchetti, J. F. Joanny, S. Ramaswamy, T. B. Liverpool, J. Prost, Madan Rao, and R. Aditi Simha. Hydrodynamics of soft active matter. *Rev. Mod. Phys.*, 85:1143–1189, Jul 2013.

[56] J.E. Marsden and T.J.R. Hughes. *Mathematical Foundations of Elasticity*. Dover, 1994.

[57] Alex Mogilner and Angelika Manhart. Intracellular fluid mechanics: Coupling cytoplasmic flow with active cytoskeletal gel. *Annual Review of Fluid Mechanics*, 50(1):347–370, 2018.

[58] Martin Michael Müller, Markus Deserno, and Jemal Guven. Interface-mediated interactions between particles: A geometrical approach. *Phys. Rev. E*, 72:061407, Dec 2005.

[59] Ali Najafi and Ramin Golestanian. Simple swimmer at low reynolds number: Three linked spheres. *Phys. Rev. E*, 69:062901, Jun 2004.

[60] Sarah A Nowak and Tom Chou. Models of dynamic extraction of lipid tethers from cell membranes. *Physical Biology*, 7(2):026002, 2010.

[61] B. Oksendal. *Stochastic Differential Equations: An Introduction*. Springer, 2000.

[62] Naomi Oppenheimer and Haim Diamant. Correlated diffusion of membrane proteins and their effect on membrane viscosity. *Biophysical Journal*, 96(8):3041–3049, April 2009.

[63] Naomi Oppenheimer and Howard A. Stone. Effect of hydrodynamic interactions on reaction rates in membranes. *Biophysical Journal*, 113(2):440–447, 2017.

[64] G. L. Paul and P. N. Pusey. Observation of a long-time tail in brownian motion. *Journal of Physics A: Mathematical and General*, 14(12):3301, 1981.

[65] Charles S. Peskin. The immersed boundary method. *Acta Numerica*, 11:1–39, July 2002.

[66] Thomas R. Powers, Greg Huber, and Raymond E. Goldstein. Fluid-membrane tethers: Minimal surfaces and elastic boundary layers. *Phys. Rev. E*, 65:041901, Mar 2002.

[67] A. Pressley. *Elementary Differential Geometry*. Springer, 2001.

[68] E. M. Purcell. Life at low reynolds number. *American Journal of Physics*, 45:3–10, 1977.

[69] François Quemeneur, Jon K Sigurdsson, Marianne Renner, Paul J Atzberger, Patricia Bassereau, and David Lacoste. Shape matters in protein mobility within membranes. *Proceedings of the National Academy of Sciences*, 111(14):5083–5087, 2014.

[70] Padmini Rangamani, Ashutosh Agrawal, KranthiK. Mandadapu, George Oster, and David. Steigmann. Interaction between surface shape and intra-surface viscous flow on lipid membranes. 12(4):833–845–, 2013.

[71] L. E. Reichl. *A Modern Course in Statistical Physics*. John Wiley and Sons, 1998.

[72] P. G. Saffman. Brownian motion in thin sheets of viscous fluid. *J. Fluid Mech.*, 73:593–602, 1976.

[73] P. G. Saffman and M. Delbruck. Brownian motion in biological membranes. *Proc. Nat. Acad. Sci. USA*, 73:3111–3113, 1975.

[74] Amaresh Sahu, Roger A. Sauer, and Kranthi K. Mandadapu. Irreversible thermodynamics of curved lipid membranes. *Phys. Rev. E*, 96:042409, Oct 2017.

[75] Jon Karl Sigurdsson and Paul J. Atzberger. Hydrodynamic coupling of particle inclusions embedded in curved lipid bilayer membranes. *Soft Matter*, 12:6685–6707, 2016.

[76] Micheal Spivak. *A Comprehensive Introduction to Differential Geometry*, volume 1. Publish or Perish Inc., 1999.

[77] H. A. Stone and L. G. Leal. The effects of surfactants on drop deformation and breakup. *Journal of Fluid Mechanics*, 220:161–186, 1990.

[78] HOWARD A. STONE and ARMAND AJDARI. Hydrodynamics of particles embedded in a flat surfactant layer overlying a subphase of finite depth. *Journal of Fluid Mechanics*, 369:151–173, 1998.

[79] Gil Tabak and Paul J. Atzberger. Stochastic reductions for inertial fluid-structure interactions subject to thermal fluctuations. *SIAM Journal on Applied Mathematics*, 75(4):1884–1914, 2015.

[80] L. N. Trefethen and D. Bau. *Numerical Linear Algebra*. Society for Industrial and Applied Mathematics, 1997.

[81] Loup Verlet. Computer "experiments" on classical fluids. i. thermodynamical properties of lennard-jones molecules. *Phys. Rev.*, 159(1):98–103, July 1967.

[82] Petia M. Vlahovska. Electrohydrodynamic instabilities of viscous drops. *Phys. Rev. Fluids*, 1:060504, Oct 2016.

[83] Xiaoguang Wang, Daniel S. Miller, Juan J. de Pablo, and Nicholas L. Abbott. Organized assemblies of colloids formed at the poles of micrometer-sized droplets of liquid crystal. *Soft Matter*, 10:8821–8828, 2014.

[84] John D. Weeks, David Chandler, and Hans C. Andersen. Role of repulsive forces in determining the equilibrium structure of simple liquids. *J. Chem. Phys.*, 54(12):5237–5247, June 1971.

[85] C. Wu, T. Fai, P. Atzberger, and C. Peskin. Simulation of osmotic swelling by the stochastic immersed boundary method. *SIAM J. Sci. Comput.*, 37(4):B660–B688, January 2015.

A. Derivations for Fluctuating Hydrodynamics on Surfaces using Vector Potentials Φ

We discuss in more detail for fluctuating hydrodynamics on the surface derivation of the stochastic dynamics of the vector potential Φ. We express the dynamics in terms of complex-valued coefficients a_s of a spherical harmonics expansion as

$$\rho \frac{\partial a_s}{\partial t} = L_s a_s + \bar{c}_s + g_s + h_s. \qquad (64)$$

The force expansion terms c_s^n are obtained from the real-space force f^n using equation 39. We obtain the stochastic driving fields g_s and h_s using a fluctuation-dissipation approach for the discretized system in a manner similar to our prior work [8, 9]. We generate Gaussian driving terms with mean zero and covariance

$$\langle g_s(t) g_{s'}(r) \rangle = -2 L_s \mathcal{C}_{ss'} \delta(t - r). \qquad (65)$$

This requires determination of the covariance $\mathcal{C}_{ss'}$ for the equilibrium fluctuations of the modes a_s.

The Gibbs-Boltzmann distribution $\rho(\mathbf{v}^\flat) = (1/Z) \exp\left(-E[\mathbf{v}^\flat]/k_B T\right)$ for the equilibrium fluctuations depends on the kinetic energy of the fluid given by

$$
\begin{aligned}
E[\mathbf{v}^\flat] &= \frac{\rho}{2} \int \langle \mathbf{v}^\flat, \mathbf{v}^\flat \rangle dA &(66)\\
&= \frac{\rho}{2} \int \langle -\star \mathbf{d}\Phi, -\star \mathbf{d}\Phi \rangle dA \\
&= \frac{\rho}{2} \int -\langle \Phi, -\boldsymbol{\delta}\mathbf{d}\Phi \rangle dA \\
&= \frac{\rho}{2} \sum_{s,s'} a_s a_{s'} \int -\langle Y_s, -\boldsymbol{\delta}\mathbf{d}Y_{s'} \rangle dA \\
&= -\frac{\rho}{2} \sum_s |a_s|^2 \lambda_s \|Y_s\|_2^2.
\end{aligned}
$$

The $s = (\ell, m)$ where ℓ is the degree and m the order. We used here the adjoint property of the co-differential $\boldsymbol{\delta}$ and the exterior derivative

d [1]. The spherical harmonics modes Y_s have L^2-norm given by $\|Y_s\|_2^2$ and are eignfunctions of the Laplace-Beltrami operator $-\boldsymbol{\delta}\mathbf{d}Y_s = \lambda_s Y_s$ with eigenvalues $\lambda_s = -\ell(\ell+1)/R^2$.

The quadratic form of the energy yields that the equilibrium fluctuations of the spherical harmonics coefficients are Gaussian with mean zero and covariance

$$\mathcal{C}_{ss'} = \langle a_s a_{s'} \rangle = \rho^{-1} k_B T |\lambda_s|^{-1} \delta_{s', \bar{s}}. \qquad (67)$$

The $\delta_{s', \bar{s}}$ denotes the Kronecker δ-function where we use notation $\bar{s} = (\ell, -m)$ to denote the conjugate mode index. The spherical harmonics coefficients are complex-valued and the field Φ must be real-valued. This requires for the coefficients $\overline{a_s} = a_{\bar{s}}$.

We generate the stochastic driving terms using $g_s = \eta_s + i\xi_s$ with $i = \sqrt{-1}$ and $\overline{g_s} = g_{\bar{s}}$ throughout. From the conditions in equation 65, we have for $m \neq 0$ that

$$\langle g_s g_{\bar{s}} \rangle = \langle g_s \overline{g_s} \rangle = \eta_s^2 + \xi_s^2 = -2 L_s \mathcal{C}_{s, \bar{s}}. \qquad (68)$$
$$\langle g_s g_s \rangle = \langle \eta_s^2 - \xi_s^2 + 2i\eta_s\xi_s \rangle = 0. \qquad (69)$$

As a consequence, we must have that $\langle \eta_s^2 \rangle = \langle \xi_s^2 \rangle$ and $\langle \eta_s \xi_s \rangle = 0$. This requires that $\langle \eta_s^2 \rangle = \langle \xi_s^2 \rangle = -L_s \mathcal{C}_{s, \bar{s}}$. The case with $m = 0$ is special since the mode is self-conjugate requiring

$$\langle g_s g_{\bar{s}} \rangle = \langle g_s g_s \rangle = \langle g_s \overline{g_s} \rangle = \eta_s^2 + \xi_s^2 = -2 L_s \mathcal{C}_{s, \bar{s}} \quad (70)$$
$$\langle g_s g_s \rangle = \langle \eta_s^2 - \xi_s^2 + 2i\eta_s\xi_s \rangle = -2 L_s \mathcal{C}_{s, \bar{s}}. \quad (71)$$

As a consequence, we must have that $\langle \xi_s^2 \rangle = 0$ and $\langle \eta_s^2 \rangle = -2 L_s \mathcal{C}_{s, \bar{s}}$.

Algorithmically, for modes $s = (\ell, m)$ these results correspond to generating g_s for $m > 0$ by computing each of the components η_s and ξ_s as independent Gaussian random variates each having the covariance $-L_s \mathcal{C}_{s\bar{s}}$, and for $m < 0$ setting $g_{\bar{s}} = \overline{g_s}$. The modes with $m = 0$ are special since they are self-conjugate and we have $g_{\bar{s}} = \overline{g_s} = \eta_s$ with covariance $-2 L_s \mathcal{C}_{s\bar{s}}$.

B. Derivation of Power-Laws for Fluctuating Hydrodynamics on a Sphere

We find the autocorelation of the fluid velocity on the spherical interface has significantly different behaviors than bulk fluids. For bulk Newtonian fluids occupying a three dimensional volume the velocity autocorrelation function has a well-known characteristic long-tail with scaling $\tau^{-3/2}$. This is supported by continuum theory [7, 12], molecular simulations [3, 23], and experimental evidence [26, 64]. In contrast, we find from equation 5 and equation 44 the interfacial fluid velocity exhibits a few different intermediate power-law scalings and exponential decay depending on the considered parameter and temporal regimes, see Figure 3. As we shall show, this arises both from the spherical geometry and from the coupling between the two-dimensional hydrodynamics and bulk surrounding three-dimensional fluid which introduce additional time-scales.

The fluid velocity is obtained from Φ as $\mathbf{v} = (-\star \mathbf{d}\Phi)^{\sharp} = v^{\theta}\partial_{\theta} + v^{\phi}\partial_{\phi}$ where $v^{\theta} = \sum_s \frac{a_s}{\sqrt{g}R}\frac{\partial Y_s}{\partial \phi}$ and $v^{\phi} = -\sum_s \frac{a_s}{\sqrt{g}R}\frac{\partial Y_s}{\partial \theta}$. The velocity autocorrelation function associated with fluctuating hydrodynamics on the sphere given in equation 5 can be expressed as

$$\left\langle v^{\theta}(0)v^{\theta}(t)\right\rangle = \sum_s \sum_{s'} \frac{\langle a_s(0)a_{s'}(t)\rangle}{|g|R^2}\frac{\partial Y_s}{\partial \phi}\frac{\partial Y_{s'}}{\partial \phi}$$
$$= \sum_s \exp(tL_s)\frac{k_B T}{|g|\rho\ell(\ell+1)}\left|\frac{\partial Y_s}{\partial \phi}\right|^2$$

$$\left\langle v^{\phi}(0)v^{\phi}(t)\right\rangle = \sum_s \sum_{s'} \frac{\langle a_s(0)a_{s'}(t)\rangle}{|g|R^2}\left|\frac{\partial Y_s}{\partial \phi}\right|^2$$
$$= \sum_s \exp(tL_s)\frac{k_B T}{|g|\rho\ell(\ell+1)}\left|\frac{\partial Y_s}{\partial \theta}\right|^2.$$
$$(72)$$

For the spherical surface, we use that the metric $|g| = R^2$. We also use that $\langle a_s^2\rangle = k_B T R^2/\rho\ell(\ell+1)$ and $\langle a_s(0)a_s(t)\rangle = \langle a_s^2\rangle \exp(tL_s)$.

We consider the autocorrelation of the fluid at a point

$$\langle \mathbf{v}(\mathbf{x},0)\cdot \mathbf{v}(\mathbf{x},t)\rangle = \left\langle v^{\theta}(0)v^{\theta}(t)\right\rangle\|\partial_{\theta}\|^2$$
$$+ \left\langle v^{\phi}(0)v^{\phi}(t)\right\rangle\|\partial_{\phi}\|^2. \quad (73)$$

Given the δ-spatial correlation of the fluctuating velocity field each of these series diverges in the limit $t \to 0$ when the full infinite expansion is taken. In practice in techniques such as the Stochastic Immersed Boundary Methods [8] the fluctuating velocity field is spatially averaged to model the dynamics of immersed particles and microstructures. This would result in fluid-structure interactions over the surface only having effectively a responses to fluid fluctuations above some critical length-scale (below some degree ℓ_*) which is related to the object's geometric size. We can obtain in practice a similar effect by working throughout with truncated series expansions with $\ell \le \ell_* = 50$ [7].

We always consider fluctuations at a point $\mathbf{x}_*$ on the equator for a given spherical coordinate chart which by symmetry yields

$$\langle \mathbf{v}(\mathbf{x}_*,0)\cdot \mathbf{v}(\mathbf{x}_*,t)\rangle = 2R^2 \left\langle v^{\phi}(0)v^{\phi}(t)\right\rangle \quad (74)$$

and

$$\left|\frac{\partial Y_s}{\partial \theta}\right|^2 = m^2 |Y_s|^2. \quad (75)$$

We can express equation 72 as

$$\left\langle v^{\phi}(0)v^{\phi}(t)\right\rangle = \sum_{\ell} \exp(tL_{\ell})\frac{k_B T}{|g|\rho\ell(\ell+1)} \cdot$$
$$\cdot \sum_{|m|\le \ell} m^2 |Y_s|^2.$$

where L_{ℓ} is given by equation 43.

We approximate these sums asymptotically to estimate significant time-scales governing different behaviors of the autocorrelation functions.

We make the ansantz throughout that we can treat the term $|Y_s|^2 \sim C$. This gives

$$\left\langle v^\phi(0)v^\phi(t) \right\rangle \approx \sum_\ell \exp(tL_\ell)\frac{k_B T}{|g|\rho\ell(\ell+1)} \cdot$$
$$\cdot \ C \sum_{|m|\leq\ell} m^2.$$

We use that $\sum_{|m|\leq\ell} m^2 = \ell(\ell+1)(2\ell+1)/3$. This very conveniently cancels the term $\ell(\ell+1)$ in the denominator that arose from the eigenvalues of the Laplace-Beltrami operator discussed in Section 2.7. After some rearrangment, we have

$$\tag{76}$$

$$\left\langle v^\phi(0)v^\phi(t) \right\rangle \approx C\frac{k_B T}{|g|\rho}\sum_\ell \left(\ell+\frac{1}{2}\right)\exp(tL_\ell).$$

We have absorbed also the additional prefactor constants into C. The spherical motion corresponding to rigid-body rotation in the bulk fluid corresponds to the mode $\ell = 1$. We see for L_ℓ only the second term (traction stress term) persists in equation 43. This gives the decay time-scale $\tau_r = 2RL/3\mu_m$ for energy dissipation through the rigid rotation of the entire spherical interface within the bulk fluid. There are two particularly interesting regimes. The first corresponds to when $R/L \gg 1$ indicating localized hydrodynamics on the surface. The second to when $R/L \ll 1$ indicating the hydrodynamics is strongly coupled nearly over the entire surface to give a response that is effectively a rigid-body rotation of the sphere.

We consider first the case when $R/L \gg 1$ and make the approximation

$$L_\ell \approx -\frac{\mu_m}{RL}\left[(\ell+\frac{1}{2}) + \epsilon\right]. \tag{77}$$

The ϵ term includes the higher-order terms. We take $\ell \ll R/L$ so that the $\ell(\ell+1)$ term does not play a significant role. We approximate the sum

using integration to obtain

$$\sum_\ell \left(\ell+\frac{1}{2}\right)\exp\left(-\frac{t\mu_m}{RL}\left(\ell+\frac{1}{2}\right)\right)$$
$$\approx \int_1^{\ell_*}\exp\left(-\frac{t\mu_m}{RL}\left(\ell+\frac{1}{2}\right)\right)\left(\ell+\frac{1}{2}\right)d\ell$$
$$= \int_{\frac{3}{2}}^{\ell_*} e^{-t\alpha\tilde\ell}\tilde\ell d\tilde\ell = \left[\frac{-1}{\alpha}e^{-\alpha t\tilde\ell}\tilde\ell\right]_{3/2}^{\tilde\ell_*}$$
$$\quad - \int_{\frac{3}{2}}^{\ell_*}\frac{-1}{\alpha t}e^{-\alpha t\tilde\ell}\tilde\ell d\tilde\ell$$
$$= \left(\frac{3}{2\alpha t} + \frac{1}{\alpha^2 t^2}\right)e^{-\frac{3}{2}\alpha t}$$
$$\approx \frac{3}{2\alpha t} + \frac{1}{\alpha^2 t^2}. \tag{78}$$

In this notation, we set $\alpha = \mu_m/RL$. We also make the assumption that $t \ll \tau_r = 2RL/3\mu_m$ so we can treat $\exp\left(-\frac{3}{2}\alpha t\right) \approx 1$. In the case with $R/L \gg 1$ and $t \ll \tau_r = 2RL/3\mu_m$, we have that

$$\left\langle v^\phi(0)v^\phi(t) \right\rangle$$
$$\approx C\frac{k_B T}{|g|\rho}\sum_\ell \left(\ell+\frac{1}{2}\right)\exp\left(-\frac{t\mu_m}{RL}(\ell+\frac{1}{2})\right)$$
$$\approx \frac{k_B T}{|g|\rho}\frac{C}{\alpha^2 t^2}. \tag{79}$$

In the case approximating with $R/L \gg 1$ followed by approximating with $\alpha = \mu_m/RL \gg 1$, we have that

$$\left\langle v^\phi(0)v^\phi(t) \right\rangle$$
$$\approx C\frac{k_B T}{|g|\rho}\sum_\ell \exp\left(-\frac{t\mu_m}{RL}(\ell+\frac{1}{2})\right)(\ell+\frac{1}{2})$$
$$\approx \frac{k_B T}{|g|\rho}\frac{3C}{2\alpha t}. \tag{80}$$

For the autocorrelation function, these results predict two distinct regimes that will exhibit different power law scalings. The first has power law t^{-2} and the second with power law scaling t^{-1}. The t^{-1} power law is consistent with prior studies of pure two dimensional fluid interfaces

predicting similar results for the long-time tail and divergence of the diffusion coefficient [3, 12]. Integrating the velocity autocorrelation functions with appropriate truncations given particle size one could obtain effective particle diffusivities within the interface using the Green-Kubo relations [32, 45, 71].

Given the coupling to the bulk surrounding fluid our fluctuating hydrodynamics have additional time-scales mediating these effects. It is interesting that even though some of our parameter regimes exhibit a t^{-1} decay this in fact only persits for a finite amount of time and is eventually mitigated by our coupling to the bulk solvent fluid. Given that finite duration, our exhibited t^{-1} decay would result in finite logrithmic terms in the diffusivity, which is consistent with Saffman-Delbrück theory which considers a similar regime [73]. Our fluctuating hydrodynamics not only capture the classical Saffman-Delbrück results but also extend this to include geometric contributions from the spherical shape and other additional time-scales in regimes where the interfacial hydrodynamics and coupling to the bulk fluid could differ significantly. Further extensions could also be made to include the temporal dynamics of the bulk solvent fluid.

We next consider the regime with $R/L \ll 1$ and make the approximation

$$L_\ell \approx \frac{\mu_m}{R^2} \left[2 - \ell(\ell+1) + \epsilon \right]. \tag{81}$$

The ϵ term includes the higher-order terms. We see a key term is $\beta = \mu_m/R^2$. In this regime we have

$$
\tag{82}
$$
$$
\sum_\ell \exp\left(\frac{t\mu_m}{R^2}(2 - \ell(\ell+1) + \epsilon) \right) (\ell + \frac{1}{2})
$$
$$
\approx \int_1^{\ell_*} \exp\left(t\beta(2 - \ell^2 - \ell) \right) (\ell + \frac{1}{2}) d\ell
$$
$$
= \int_1^{\ell_*} \exp\left(-t\beta(\ell + \frac{1}{2})^2 \right) (\ell + \frac{1}{2}) d\ell \exp(t\beta \frac{9}{4})
$$
$$
= \left[\exp\left(-t\beta(\ell + \frac{1}{2})^2 \right) \left(-\frac{1}{2t\beta} \right) \right]_1^{\ell_*} \exp(t\beta \frac{9}{4})
$$
$$
= \exp(-t\beta \frac{9}{4}) \exp(t\beta \frac{9}{4}) \left(\frac{1}{2t\beta} + (\text{small terms}) \right)
$$
$$
\approx \frac{1}{2\beta t}.
$$

We obtained these results using completion of the square in the exponent.

In the regime with $R/L \ll 1$, we see the velocity autocorrelation has

$$
\tag{83}
$$
$$
\left\langle v^\phi(0) v^\phi(t) \right\rangle
$$
$$
\approx \frac{k_B T}{|g|\rho} C \sum_\ell \exp\left(-\frac{t\mu_m}{R^2}(2 - \ell(\ell+1) + \epsilon) \right) (\ell + \frac{1}{2})
$$
$$
\approx \frac{k_B T}{|g|\rho} \frac{C}{2\beta t}.
$$

This predicts a power law decay with scaling t^{-1}.

We see that the relaxation time-scale τ_r for some systems can be quite large relative to the other time-scales. In these regimes, we find something interesting can occur where the velocity autocorrelation function plateaus. This is predicted by our theory to occur in the regime when the time t satisfies $\tau_a = R^2/4\mu_m \ll t \ll \tau_r = 2RL/3\mu_m$. In this regime, the correlations associated with the internal flow of the hydrodynamics within the interfacial decays rapidly to zero. However, the rigid rotational motion of the entire fluid interface can still persist for awhile until the rotation reaches its decay time-scale that dissipates this motion. This leads to the interesting

plateaus seen in the velocity autocorrelation function in Figure 3. We also see that for all non-zero parameter choices the autocorrelation function will eventually exhibit an exponential decay when reaching time-scale $t \gg \tau_r = 2RL/3\mu_m$. This is a consequence of the rigid-body rotational mode $\ell = 1$ being the longest lived mode and eventually dissipating energy from the interfacial fluid to the bulk surrounding fluid. Our calculations show that surface fluctuating hydrodynamics on quasi two dimensional fluid interfaces can exhibit significantly different phenomena relative to their bulk counter-parts in three dimensional space.

C. Spherical Harmonics

We expand functions Φ on the surface using the spherical harmonics

$$\Phi(\theta, \phi) = \sum_{n=0}^{\infty} \sum_{m=-n}^{n} \hat{\Phi}_n^m Y_n^m(\theta, \phi), \qquad (84)$$

where

$$\begin{aligned} Y_n^m(\theta, \phi) &= \sqrt{\frac{(2n+1)(n-m)!}{4\pi(n+m)!}} \cdot \\ &\quad \cdot P_n^m(\cos(\phi)) \exp(im\theta). \end{aligned} \qquad (85)$$

The m denotes the order and n the degree for $n \geq 0$ and $m \in \{-n, \ldots, n\}$. The P_n^m denote the *Associated Legendre Polynomials*. We denote by θ the azimuthal angle and by ϕ the polar angle of the spherical coordinates [6]. We work with real-valued functions and use that modes are self-conjugate in the sense $Y_n^m = \overline{Y_n^{-m}}$.

We can express the spherical harmonic modes as

$$Y_n^m(\theta, \phi) = X_n^m(\theta, \phi) + iZ_n^m(\theta, \phi). \qquad (86)$$

The X_n^m and Z_n^m denote the real and imaginary parts. We use this splitting in our numerical methods to construct a purely real set of basis functions on the unit sphere with maximum degree N which consists of $(N+1)^2$ basis elements.

For the case $N = 2$ we have the basis elements

$$\begin{aligned} &\tilde{Y}_1 = Y_0^0, \ \ \tilde{Y}_2 = Z_1^1, \ \ \tilde{Y}_3 = Y_1^0, \ \ \tilde{Y}_4 = X_1^1, \\ &\tilde{Y}_5 = Z_2^2, \ \ \tilde{Y}_6 = Z_2^1, \ \ \tilde{Y}_7 = Y_2^0, \ \ \tilde{Y}_8 = X_2^1, \\ &\qquad\qquad\qquad\qquad\qquad \tilde{Y}_9 = X_2^2. \end{aligned} \qquad (87)$$

Similar conventions are used for the basis for the other values of N. We take final basis elements Y_i that are normalized as $Y_i = \tilde{Y}_i / \sqrt{\langle \tilde{Y}_i, \tilde{Y}_i \rangle}$.

Derivatives are used within our finite expansions by evaluating analytic formulas whenever possible for the spherical harmonics in order to try to minimize approximation error [6]. Approximation errors are incurred when sampling the values of expressions involving these derivatives at the Lebedev nodes and when performing quadratures [49]. The derivative of the spherical harmonics in the azimuthal coordinate θ is given by

$$\begin{aligned} \partial_\theta Y_n^m(\theta, \phi) &= \partial_\theta \sqrt{\frac{(2n+1)(n-m)!}{4\pi(n+m)!}} \cdot \\ &\quad \cdot P_n^m(\cos(\phi)) \exp(im\theta) \\ &= imY_n^m(\theta, \phi). \end{aligned} \qquad (88)$$

We see this has the useful feature that the derivative in θ of a spherical harmonic of degree n is again a spherical harmonic of degree n. As a consequence, we have in our numerics that this derivative can be represented in our finite basis. This allows us to avoid additional L^2 projections allowing for computation of the derivative in θ without incurring an approximation error. The derivative of the spherical harmonics in the polar angle ϕ is given by

$$\begin{aligned} \partial_\phi Y_n^m(\theta, \phi) &= m \cot(\phi) Y_n^m(\theta, \phi) \\ &\quad + \sqrt{(n-m)(n+m+1)} \cdot \\ &\quad \cdot \exp(-i\theta) Y_n^{m+1}(\theta, \phi). \end{aligned} \qquad (89)$$

We see that unlike derivatives in θ the derivative in ϕ can not be represented in general in terms of a finite expansion of spherical harmonics. In our

numerics, we use the expression in equation 89 for $\partial_\phi Y_n^m(\theta, \phi)$ when we need to compute values at the Lebedev quadrature nodes. These analytic results provide a convenient way to compute derivatives of differential forms following the approach discussed in our prior paper [33]. By using these analytic expressions, we have that the subsequent hyperinterpolation of the resulting expressions are where the approximation errors are primarily incurred. Throughout our discussions to simplify the notation we use the convention that $Y_n^m = 0$ when $m \geq n+1$. Further discussion of spherical harmonics can be found [6]. Further discussions about how we use the spherical harmonics in our numerical calculations of exterior calculus operators also can be found in our papers [33, 75].

D. Exterior Calculus: Coordinate Expressions

We expressed operators on the surface using exterior calculus. We give here explicit expressions in coordinates for these operators. Since there is no global non-singular coordinate system on the sphere, we ensure numerical accuracy by switching between two coordinate charts. In chart A we have coordinates $(\hat{\theta}, \hat{\phi})$ with singularities at the north and south poles. In chart B we have coordinates $(\tilde{\theta}, \tilde{\phi})$ having singularities at the east and west poles. To avoid issues with singularities when seeking a value at a point $\mathbf{x}$, we evaluate expressions within each chart in the regions with $\pi/4 \leq \phi \leq 3\pi/4$ and $\pi/4 \leq \tilde{\phi} \leq 3\pi/4$. We give all expressions with generic polar coordinates (θ, ϕ) which we subsequently use in practice in our numerical calculations by choosing the appropriate chart A or chart B. More details on our approach can also be found in [75].

The exterior derivatives can be expressed for a 0-form f and 1-form $\boldsymbol{\alpha}$ as

$$
\begin{aligned}
\mathbf{d}f &= (\partial_\theta f)\mathbf{d}\theta + (\partial_\phi f)\mathbf{d}\phi = f_\theta \mathbf{d}\theta + f_\phi \mathbf{d}\phi \\
\mathbf{d}\alpha &= (\partial_\theta \alpha_\phi - \partial_\phi \alpha_\theta)\mathbf{d}\theta \wedge \mathbf{d}\phi.
\end{aligned}
\tag{90}
$$

The generalized curl on the radial manifold of a 0-form and 1-form can be expressed as

$$
\begin{aligned}
-\star \mathbf{d}f &= \mathrm{curl}_\mathcal{M}(f) \\
&= \sqrt{|g|} \left(f_\theta g^{\theta\phi} + f_\phi g^{\phi\phi} \right) \mathbf{d}\theta \\
&\quad - \sqrt{|g|}(f_\theta g^{\theta\theta} + f_\phi g^{\phi\theta})\mathbf{d}\phi \quad (91) \\
-\star \mathbf{d}\alpha &= \mathrm{curl}_\mathcal{M}(\boldsymbol{\alpha}) = \frac{\partial_\phi \alpha_\theta - \partial_\theta \alpha_\phi}{\sqrt{|g|}}. \quad (92)
\end{aligned}
$$

In this notation we have taken the conventions that $f_j = \partial_{x^j} f$ and α_j such that $\boldsymbol{\alpha} = \alpha_j \mathbf{d}x^j$ where $j \in \{\theta, \phi\}$. The isomorphisms $\sharp$ and $\flat$ between vectors and co-vectors can be expressed explicitly as

$$
\begin{aligned}
\mathbf{v}^\flat &= (v^\theta \boldsymbol{\sigma}_\theta + v^\phi \boldsymbol{\sigma}_\phi)^\flat \quad (93) \\
&= v^\theta g_{\theta\theta}\mathbf{d}\theta + v^\theta g_{\theta\phi}\mathbf{d}\phi + v^\phi g_{\phi\theta}\mathbf{d}\theta + v^\phi g_{\phi\phi}\mathbf{d}\phi \\
&= (v^\theta g_{\theta\theta} + v^\phi g_{\phi\theta})\mathbf{d}\theta + (v^\theta g_{\theta\phi} + v^\phi g_{\phi\phi})\mathbf{d}\phi
\end{aligned}
$$

$$
\begin{aligned}
(\boldsymbol{\alpha})^\sharp &= (\alpha_\theta \mathbf{d}\theta + \alpha_\phi \mathbf{d}\phi)^\sharp \quad (94) \\
&= \alpha_\theta g^{\theta\theta}\boldsymbol{\sigma}_\theta + \alpha_\theta g^{\theta\phi}\boldsymbol{\sigma}_\phi + \alpha_\phi g^{\phi\theta}\boldsymbol{\sigma}_\theta + \alpha_\phi g^{\phi\phi}\boldsymbol{\sigma}_\phi \\
&= (\alpha_\theta g^{\theta\theta} + \alpha_\phi g^{\phi\theta})\boldsymbol{\sigma}_\theta + (\alpha_\theta g^{\theta\phi} + \alpha_\phi g^{\phi\phi})\boldsymbol{\sigma}_\phi
\end{aligned}
$$

We use the notational conventions here that for the embedding map $\boldsymbol{\sigma}$ for spherical coordinates in $\mathbb{R}^3$ we have $\boldsymbol{\sigma}_\theta = \partial_\theta$ and $\boldsymbol{\sigma}_\phi = \partial_\phi$. Combining the above equations we can express the generalized

curl as

$$(95)$$

$$
\begin{aligned}
(-\star \mathbf{d}f)^\sharp &= ([\sqrt{|g|}(f_\theta g^{\theta\phi} + f_\phi g^{\phi\phi})]g^{\theta\theta} \\
&+ [-\sqrt{|g|}(f_\theta g^{\theta\theta} + f_\phi g^{\phi\theta})]g^{\phi\theta})\boldsymbol{\sigma}_\theta \\
&+ ([\sqrt{|g|}(f_\theta g^{\theta\phi} + f_\phi g^{\phi\phi})]g^{\theta\phi} \\
&+ [-\sqrt{|g|}(f_\theta g^{\theta\theta} + f_\phi g^{\phi\theta})]g^{\phi\phi})\boldsymbol{\sigma}_\phi \\
&= \frac{f_\phi}{\sqrt{|g|}}\boldsymbol{\sigma}_\theta - \frac{f_\theta}{\sqrt{|g|}}\boldsymbol{\sigma}_\phi
\end{aligned}
$$

$$(96)$$

$$
\begin{aligned}
-\star \mathbf{d}\mathbf{v}^\flat &= -\frac{\partial_\phi(v^\theta g_{\theta\theta} + v^\phi g_{\phi\theta})}{\sqrt{|g|}} \\
&+ \frac{\partial_\theta(v^\theta g_{\theta\phi} + v^\phi g_{\phi\phi})}{\sqrt{|g|}}.
\end{aligned}
$$

The scalar Laplace-Beltrami operator $\Delta_{LB} =$ $-\boldsymbol{\delta}\mathbf{d}$ that acts on 0-forms can be expressed in coordinates as

$$\Delta_{LB} = -\boldsymbol{\delta}\mathbf{d} = \frac{1}{\sqrt{|g|}}\partial_i \left(g^{ij}\sqrt{|g|}\partial_j\right). \quad (97)$$

The g_{ij} denotes the metric tensor, g^{ij} the inverse metric tensor, and $|g|$ the determinant of the metric tensor.

We also mention that the velocity field of the hydrodynamic flows $\mathbf{v}$ is recovered from the vector potential Φ as $\mathbf{v}^\flat = -\star \mathbf{d}\Phi$. We obtain the velocity field $\mathbf{v} = \mathbf{v}^\sharp = (-\star \mathbf{d}\Phi)^\sharp$ using equation 95. Similarly from the force density $\mathbf{b}$ acting on the fluid, we obtain the data $-\star \mathbf{d}\mathbf{b}^\flat$ for the vector potential formulation of the hydrodynamics using equation 96. Additional details and discussions of these operators also can be found in our related papers [33,75] and in [1,67,76].